

EXPERIMENTAL DEMONSTRATION OF
TRANSMISSION ENHANCEMENT
THROUGH SUBWAVELENGTH APERTURES
AT MICROWAVE FREQUENCIES

A THESIS
SUBMITTED TO THE DEPARTMENT OF
ELECTRICAL AND ELECTRONICS ENGINEERING
AND THE GRADUATE SCHOOL OF ENGINEERING AND SCIENCES
OF BILKENT UNIVERSITY
IN PARTIAL FULLFILMENT OF THE REQUIREMENTS
FOR THE DEGREE OF
MASTER OF SCIENCE

By
DAML ATEŞ
June 2012

I certify that I have read this thesis and that in my opinion it is fully adequate, in scope and in quality, as a thesis for the degree of Master of Science.

Prof. Dr. Ekmel Özbay (Supervisor)

I certify that I have read this thesis and that in my opinion it is fully adequate, in scope and in quality, as a thesis for the degree of Master of Science.

Prof. Dr. Ayhan Altıntaş

I certify that I have read this thesis and that in my opinion it is fully adequate, in scope and in quality, as a thesis for the degree of Master of Science.

Assoc. Prof. Dr. Hamza Kurt

Approved for the Graduate School of Engineering and Sciences:

Prof. Dr. Levent Onural

Director of Graduate School of Engineering and Sciences

ABSTRACT
EXPERIMENTAL DEMONSTRATION OF
TRANSMISSION ENHANCEMENT THROUGH
SUBWAVELENGTH APERTURES
AT MICROWAVE FREQUENCIES

Damla Ateş
M.S. in Electrical and Electronics Engineering
Supervisor: Prof. Dr. Ekmel Özbay

June 2012

Metamaterials are artificial materials with novel electromagnetic characteristics. They are used in many applications including imaging, super lenses, cloaking, transmission enhancement, beaming and recently in nano applications. One of the major building blocks is the split ring resonators (SRR). We can construct metamaterials by using a single or an array of the SRRs.

In this thesis, enhanced transmission through subwavelength apertures, which is one of the applications of metamaterials, is obtained by using various split ring resonators configurations. We demonstrated transmission enhancement with Connected Split Ring Resonators (CSRRs), Omega-like Split Ring Resonators and Stack-like Split Ring Resonators through circular and rectangular subwavelength apertures experimentally and numerically at the microwave frequencies. We report the highest experimental transmission enhancement results in the literature so far. Besides high factors, we also obtained multi-peak resonant characteristics with Stack-like SRR designs.

Furthermore, we analyzed these various SRR samples numerically in order to understand the resonance behavior. We also discuss the effects of shorting the loops, omitting the components of the SRRs and aperture geometry to the resonance frequency. Finally, we applied Tight Binding methods to analyze the multi-peak characteristics of the Stack-like SRR design.

Keywords: Metamaterial, Split Ring Resonator, Transmission Enhancement, Diffractions and Gratings, Subwavelength apertures.

ÖZET

MİKRODALGA FREKANSLARINDA
DALGABOYU-ALTI DELİKLERDEN OLAĞANÜSTÜ
ELEKTROMANYETİK GEÇİRGENLİĞİN DENEYSEL
GÖSTERİMİ

Damla Ateş
Elektrik ve Elektronik Mühendisliği Bölümü Yüksek Lisans
Tez Yöneticisi: Prof. Dr. Ekmel Özbay
Haziran 2012

Metamalzemeler, farklı elektromanyetik karakteristiğe sahip yapay yollarla elde edilen malzemelerdir. Metamalzemeler, görüntüleme, süper lensler, görünmezlik pelerini, olağanüstü elektromanyetik geçirgenlik, nanoteknolojik yapılar gibi birçok alanda kullanılırlar. Metamalzemelerin en küçük yapıtaşlarından biri de *Ayrık Halkalı Rezonatörler*dir (SRR). Bu ayrık halkalı rezonatörleri tek başlarına ya da bir dizi halinde kullanarak çeşitli metamalzemeler elde edebiliriz.

Bu çalışmada, Bağlı Ayrık Halkalı Rezonatörler, Omega tipi Ayrık Halkalı Rezonatörler ve Sıralı Ayrık Halkalı Rezonatörler yardımıyla dairesel ve dikdörtgensel dalga-boyu altı deliklerden, mikrodalga frekanslarında olağanüstü elektromanyetik geçirgenlik sağladık. Deneyleerde elde ettiğimiz sonuçlar şu ana kadar elde edilmiş sonuçların hepsinden daha yüksektir. Yüksek elektromanyetik geçirgenliğin yanısıra, Sıralı Ayrık Halkalı Rezonatörler sayesinde daha geniş bir band aralığında geçirgenlik kazandık.

Deneyleerin yanısıra elektromanyetik geçirgenliğe sebep olan rezonansları anlamak için nümerik analizler yaptık. Nümerik analizlerin deneysel sonuçlarla örtüşüğünü gözlemledik. Son olarak, bu yapılarda çeşitli geometrik değişikliklerle analizler yaptık. Sıralı Ayrık Halkalı Rezonatörler'in elektromanyetik geçirgenliğini anlamak için Tight Binding methodunu kullandık.

Anahtar kelimeler: Metamalzemeler, Ayrık Halkalı Rezonatörler, Olağanüstü Elektromanyetik geçirgenlik, arttırılmış iletim, Kırınım, Dalgaboyu altı delikler.

Acknowledgements

First of all, it is my pleasure to express my deepest gratitude and respect to my supervisor Prof. Ekmel Özbay for his invaluable guidance, ideas, encouragement and endless support during my thesis and my entire academic life. He supported me at every single stage of my academic career and gave me a chance to make dreams come true.

I would like to thank to the members of my thesis committee, Prof. Ayhan Altıntaş and Assoc. Prof. Hamza Kurt for their guidance and commenting on the thesis.

I am very lucky to be a member of Nanotam, where I found best friends and colleagues. I would like to thank Özgür Çakmak, Evrim Çolak, and Andriy Serebryannikov for their help and contributions to joint works during my thesis. Especially, I would like to thank my close friends who are also the greatest office mates, Semih Çakmakyapan and Neval Cinel for their intellectual and moral support during my research and thesis. They helped and supported me whenever I struggle. Also, I would like to thank Gülesin Eren, Serdar Ögüt for being such good friends and Nursel Aşıcı, Gamze Seymenoğlu and to all Nanotam members.

I am very grateful to my instructors, especially Prof. Hitay Özbay, Assoc. Prof. Aykutlu Dana, Prof. Orhan Aytür and all the other EEE faculty members for their assistance during my undergraduate and graduate studies. I would like to thank to my friends Erdem Ulusoy and Olgu Çalimli, and senior Mürüvet Parlakay and all my friends in EEE department.

I owe thanks to my friends Özlem İskender, Seher Acer, Türkiz Erdoğan, Dilce Gözüyaşlı, Elif Demirli, Gizem Altay, and Ayşe Yeşil for their endless support and being such good friends to me. Also, I especially thank to my late friend Deniz Aksoy for his intellectual and moral support and pure friendship. We miss you so much and we will always remember you.

Special thanks go to my mother, my father, my grandmother, and to all of my family for their boundless love, support, encouragement and understanding during my research and thesis. I am a very lucky person to have a great family.

Finally, I would like to thank to Üstun Özgür for his endless support, help and love.

To my mother Raziye and father Ergün

Table of Contents

List of Figures	ix
List of Tables	xii
Chapter 1 Introduction	1
Chapter 2 Theoretical Background	4
2.1 Split Ring Resonators	4
2.2 Transmission Enhancement Phenomenon	5
Chapter 3 Transmission Enhancement using Connected Split Ring Resonators	8
3.1 CSRR Design and Experimental Environment.....	9
3.2 Measurement and Simulation Results	13
Chapter 4 Transmission Enhancement using Omega-like Split Ring Resonators	24
4.1 Omega-like Split Ring Resonator designs	25
4.2 Experimental Environment.....	26
4.3 Transmission Enhancement Results	27
4.4 Verification of Experiments through Simulations.....	30
4.5 Physical Analysis of Transmission Enhancement via Omega-like SRRs	30
4.6 Parametrical Analysis that Strengthen the Physical Observations	32
Chapter 5 Transmission Enhancement using Stack-like Split Ring Resonators	37
5.1 Multi-Stack Design and SRR configuration	38
5.2 Experimental Environment of the Stacked Metal Screens with SRRs and Transmission Spectra	41
5.3 Physical Analysis and Tight Binding Calculations	48
Chapter 6 Conclusion	54
Bibliography	57

List of Figures

Figure 2.1: Schematics of a single SRR with geometric parameters of splits, metal width and radius [12].	4
Figure 2.2: Diffraction and transmission spectrum of the light through subwavelength aperture (Genet et al.) [15].	5
Figure 3.1: SRR coupled subwavelength aperture in the metallic screen design introduced by Aydin et al. [38].	8
Figure 3.2: Single SRR configurations (a) Rectangular SRR, SRRB and (b) Circular SRR, SRRB.	9
Figure 3.3: SRRB and SRRB samples in order to design CSRR samples: Sample A and Sample B.	10
Figure 3.4: Simulated Transmission spectra of (a) SRRB and Sample A, (b) SRRB and Sample B.	11
Figure 3.5: Sample A incorporated in the aperture.	12
Figure 3.6: Design of the experimental setup.	13
Figure 3.7: Measured Transmitted Intensity through (a) Sample A (solid red line) and Single Aperture (solid black line) and (b) Sample B (solid red line) and Single Aperture (solid black line).	14
Figure 3.8: Calculated Enhancement Factors from measurement results for (a) Sample A and (b) Sample B.	15
Figure 3.9: Fabricated Samples (a) Sample A, (b) Sample B and (c) Experimental setup.	15
Figure 3.10: Simulated Transmission Intensity Spectra for (a) Sample A (solid red line) and Single Aperture (solid black line), (b) Sample B (solid red line) and Single Aperture (solid black line).	16
Figure 3.11: Simulated Transmitted Electric Fields Results corresponding to transmission through Single Aperture incorporated with Sample B (dashed red line), Inner Rings shorted Sample B (solid green line), and Outer Rings shorted Sample B (dashed black line).	17
Figure 3.12: STE factor for various radii in the range 2.4-7 mm where the black dots are the numerical results and red line is experiment organized by Cakmak et al. [39].	19
Figure 3.13: (a) Simulated transmitted electric field through Big CSRR in the small aperture (black line) and Big CSRR in the big aperture (red line), (b) Simulated Field Enhancement of Big CSRR through the small aperture (black line) and the big aperture (red line).	20

Figure 3.14: (a) Simulated transmitted electric field of Sample A (red line), Sample A PRL design (green line) and Sample A without Connecting bars (b) Simulated Field enhancement of of Sample A (red line), Sample A PRL design (green line) and Sample A without connecting bars	21
Figure 3.15: (a) Induced surface currents when the CSRR is excited, (b) Field localization around the aperture, Electric field localization in the vicinity of the aperture when the CSRR is (c) without connecting bars, (d) with connecting bars.....	22
Figure 4.1: Omega samples when (a) deposited both sides, (b) an array that includes three Omega Samples, (c) a periodic array in both sides, (d) example of a transmission spectrum.	24
Figure 4.2: a) Schematic of the designed omega-like split-ring resonators from the front side where the parameters are $r = 3$ mm, $w = 1$ mm, and $l = 4$ mm. (b) Designed omega-like split ring resonator from the back side. (c) Copper screen with omega-like split-ring resonators inserted in the circular aperture where the dimensions are $h = 7.5$ mm and $L = 700$ mm. (d) Copper screen with omega-like split-ring resonators inserted in the rectangular aperture.....	26
Figure 4.3: Schematic demonstration of the transmission enhancement experiments using waveguide antennas and HP8510C network analyzer.	27
Figure 4.4: (a) Experimental and (b) simulation results of the transmission intensity (dB) through the circular aperture (c) experimental and (d) simulation results for the rectangular aperture (solid black line is for the single aperture, solid red line is for the omega-like split-ring resonators inserted across aperture.)	28
Figure 4.5: Enhancement factor in the case of the omega-like split-ring resonators inserted (a) across the circular aperture and (b) across the rectangular aperture.	29
Figure 4.6 Surface current density (a) at 3.15 GHz (even mode operation) where the first enhancement peak occurs, (b) at 3.95 GHz (odd mode operation) where second enhancement peak occurs, (c) at 5.00 GHz (non-resonant frequency) where no enhancement occurs.	31
Figure 4.7 (a) Difference of the transmission through circular and rectangular apertures and (b) difference of the enhancement factor when omega-like split-ring resonators are inserted across circular and rectangular apertures.....	32
Figure 4.8: Electric Field Distribution maps of the (a) Double-sided Omega-like SRR across the rectangular aperture at 3.95 GHz (above), 5.00 GHz (below), (b) Single-sided Omega-like SRR across the rectangular aperture at 3.95 GHz (above), 5.00 GHz (below), (c) Rectangular Aperture without Omega-like SRR at 3.95 GHz (above), 5.00 GHz (below).	33
Figure 4.9: (a) Transmission characteristics of Double-sided (Solid Red), Single-sided Omega-like SRRs (Solid Blue), Aperture without Omega-like SRRs (Solid Black), (b), (c) and (d)	

Electric Field Distribution Maps collected at 3.95 GHz (Resonance Frequency) respectively.....	35
Figure 4.10: Field Distribution Maps (a) 0.1λ away (b) 0.5λ away, (c) 0.7λ away from Omega- like SRR, and (d) Normalized transmitted intensity versus distance away from the Omega- like SRR in terms of operational wavelength.	36
Figure 5.1: Simulation environment of Four Stacked-Four SRR design (a) from the side, (b) from the front perspective.	38
Figure 5.2: (a) and (b) various configurations of SRR coupled single aperture designed by Aydin et al. and Cakmak et al. (c) SRR design from the front view [38, 39].	39
Figure 5.3: SRR design that is used to couple the stacks.	40
Figure 5.4: (a) SRR cover the half of the aperture, (b) zoomed view from the front side, and (c) zoomed view from the back side.	41
Figure 5.5: Transmission spectra of the SRR incorporated single aperture (red solid line) and single aperture (black solid line).	42
Figure 5.6: Transmission spectra of the two Stacks with two SRRs (red solid line) and two stacks without SRRs (black solid line).....	43
Figure 5.7: Transmission spectra of the three Stacks with three SRRs (red solid line) and three stacks without SRRs (black solid line).	44
Figure 5.8: Transmission spectra of the four Stacks with four SRR (red solid line) and four stacks without SRRs (black solid line).	45
Figure 5.9: Calculated enhancement factors of single stack-SRR (solid black line), two stacks- two SRRs (dashed red line), three stacks-three SRRs (solid blue line), four stacks-four SRRs (solid green line).	46
Figure 5.10: Simulated Transmission Spectra of single stack-SRR (solid black line), two stacks- two SRRs (dashed red line), three stacks-three SRRs (solid blue line), four stacks-four SRRs (solid green line).	47
Figure 5.11: Simulated Transmission spectrum of the ten stack-ten SRRs system with showing the enhanced band gap $\Delta\omega$	53

List of Tables

Table 5.1: Calculated and measured values of resonant frequencies for the Three Stack –Three SRR system.	50
Table 5.2: The calculated and simulated values of resonant frequencies for the Three Stack – Three SRR system.	51

Chapter 1

Introduction

Electromagnetism has taken a fundamental role in our lives. Electromagnetic applications are used widely in many areas including imaging, antenna engineering, perfect lenses, cloaking, optics and photonics.

One of the main research topics in electromagnetism is electromagnetic propagation. To improve electromagnetic propagation, antennas and waveguides, have been designed. Propagation characteristics such as transmission, reflection and diffraction are the major research issues in this topic. Depending on goals, their effects need to be improved or reduced.

Another significant topic in electromagnetism is the light matter interaction. There is an interaction between the matter and electromagnetic wave that dominates the propagation characteristics. Therefore; one needs to understand the light-matter or wave-matter interaction to control electromagnetic propagation.

The magnetic response of a material to a wave is determined by its dielectric permittivity (ϵ) and magnetic permeability (μ). For materials found in nature, ϵ and μ are usually positive. However, their responses can be changed by redesigning them artificially. These redesigned materials are defined as *metamaterials*. The term “meta” is adopted from Greek which means “beyond”.

Similar to materials consist of atoms, the basic building blocks of metamaterials are meta-atoms that are smaller than the operational wavelength. Metamaterials are one of the most interesting artificial materials nowadays because of their controllable electromagnetic parameters (ϵ and μ) obtained by modifying the geometry of their designs. Their parameters can be adjusted to desired negative and positive values.

Even before the term “*metamaterials*” was defined, electromagnetic parameters had already become a research topic. In 1968, Russian physicist Victor

CHAPTER 1. INTRODUCTION

Veselago proposed that ϵ and μ can in fact be negative in his famous paper “The electrodynamics of substances with simultaneously negative values of ϵ and μ ” [1]. Veselago named such materials “Left-Handed Materials”. Less than half a decade later, this phenomenon was realized by another renowned theoretical physicist Sir John Pendry, who showed how such materials could be constructed [2]. Electromagnetic parameters determine the index of refraction and their simultaneously negative behavior generates a negative index of refraction.

For guiding and beaming the incident electromagnetic waves, beside metamaterials, other optical applications such as photonic crystals, metallic grating structures and fiber-modeled waveguides are used. Furthermore; to obtain strong waveguiding and beaming through transmission, plasmonic effects can be exploited [3-5].

Metamaterials with these magical properties have gained an increasing attention in the scientific community and have found use in many applications including perfect lenses that are capable of imaging subwavelength sized substances with a high resolution, magnifying hyper lenses, and cloaking applications that work in the microwave regime [6-9]. In addition, metamaterials are scalable materials that we can tailor for the desired frequency of range such as radio, microwave, millimeter-wave, infrared (IR), visible wavelengths [10, 11]; so they have a wide range of applicability.

In this research, we investigate alternative ways to obtain a better and controllable transmission via various metamaterial configurations. We seek the optimal design that enhances transmission and surpasses the results reported in literature. The principle reason that we use metamaterials is their easily tailored and characterized. Hence, we can anticipate the results and demonstrate their validity through the experiments at the desired regime. We also verify the experiments with numerical analysis and explain their physical behind them.

In Chapter 2, we introduce the main building blocks of metamaterials which called Split Ring Resonators (SRRs). We also explain their magnetic resonance behavior, introduce the transmission enhancement phenomenon and discuss the previous related work in the literature.

CHAPTER 1. INTRODUCTION

In Chapter 3, we propose a way to increase the transmission and obtain an enhancement. We describe our novel SRR design called Connected Split Ring Resonators (CSRR). We demonstrate the transmission enhancement by experiments and numerical analysis. We analyze further why transmission enhancement occurs.

Chapter 4 is similar to Chapter 3, however, instead of CSRR, we use another metamaterial that we designed called Omega-like SRR. Using this design, we show that a greater transmission enhancement occurs.

In Chapter 5, our aim is to obtain a transmission enhancement in a wide-range multi-peak resonance system. To achieve this, we design a stack-like SRR structure in which large metal plates with SRRs are placed in succession and aligned. Using this design, we obtain an enhancement in a broader bandwidth. Finally, we apply the Tight Binding (TB) approximation to analyze the physical origins of the enhanced multi-peak resonance system.

We conclude in Chapter 6 and summarize our findings and future works.

Chapter 2

Theoretical Background

In this chapter, we briefly introduce the Split Ring Resonators and transmission enhancement phenomenon.

2.1 Split Ring Resonators

In 1999, Pendry et al. proposed an alternative way to change the magnetic permeability to negative by designing a periodic array of conducting particles. Since then these periodic arrays also known as SRRs became a hot topic.

To understand the resonant behavior of the SRRs, we should consider its design first. The conventional SRR is shown in Figure 2.1 [12].

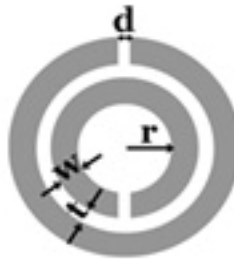


Figure 2.1: Schematics of a single SRR with geometric parameters of splits, metal width and radius [12].

In this design, the conducting wires acts as inductors; the splits and gaps assume capacitive roles (capacitors). From a circuit theory point of view, this LC composition creates a resonant behavior. Hence, the magnetic resonance gains negative and positive values around the resonance frequency.

The structure in Figure 2.1 is used as the unit cell of a periodic array. A single unit also has a resonant behavior, however, to have band gap more observable, we need to use a periodic array of this structure in three dimensions [13].

2.2 Transmission Enhancement Phenomenon

Electromagnetic power transmission through holes has been a significant research topic. The most significant contribution was done by H. Bethe. He considered the case of power transmission through a small aperture drilled in an opaque or metallic screen. In 1944, he analyzed the relation between the transmission efficiency and the dimension of the aperture (radius, r) compared to operational wavelength (λ) [14]. He proposed that transmission efficiency is proportional $(r/\lambda)^4$. Figure 2.2 shows the behavior that the Bethe has proposed [15].

As shown in the figure, the power transmission becomes extremely low at small apertures. However, it can be controlled in both intensity and frequency by modifying the geometry of the small aperture.

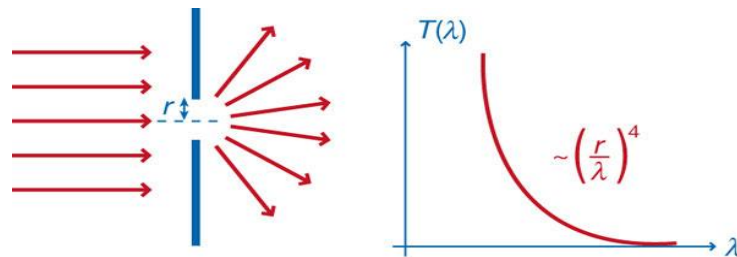


Figure 2.2: Diffraction and transmission spectrum of the light through subwavelength aperture (Genet et al.) [15].

Ebbesen and other scientists have since work on this topic that Bethe has started, trying to improve the efficiency of transmission [16]. Those studies, in which transmission has been enhanced beyond the limit proposed by Bethe, have been named “*extraordinary transmission*”. In those studies, an array of hole was drilled on a metallic screen. Due to surface plasmon phenomenon, more efficient transmission than Bethe’s predictions at specific frequencies was achieved. The extraordinary transmission topic gained an attention by other research groups and various results were obtained both theoretically [17-20] and experimentally [21-27].

CHAPTER 2. THEORETICAL BACKGROUND

Wave and metallic screen interaction was investigated from the surface plasmon polariton point of view and the transmission efficiency was analyzed in this manner. It was showed that the surface plasmons of the metallic screen interact with the incident photons [24, 25, 27]. Especially if periodic designs are used the number of interactions increases because these interactions occur for every single subwavelength structure and hole each of which act like point sources and consequently, transmission efficiency increases. Finally it should be noted that, although periodic designs are more advantageous as shown, the transmission through single aperture still remains as a challenge and has been analyzed by other physicists [28-31].

It has been shown that it is also possible to support the surface plasmons by adding particular corrugations to the surfaces. In the first earlier studies, corrugations were added to single apertures. It is possible to create a grating-like structure by adding periodic corrugations around these single apertures. The Bull's eye design is an example of a corrugation-hole structure [4]. The studies showed that the transmission through the single aperture increases remarkably and the beaming can be controlled [3-5]. Later on, the same technique was applied to other periodic designs [32, 33]. The incident beam is coupled to these periodic grooves or corrugations.

Pendry and his colleagues have also shown that the surface plasmons exist not only in the optical regime but also in the microwave frequencies as “spoof plasmons”. Spoof plasmons support the coupling that enhances transmission [34, 35].

After Pendry's and Ebbesen's observations regarding the corrugated surfaces, other scientists including Alu et al. and Marques et al. investigated the effect of using metamaterial slabs with SRRs as corrugations [36, 37]. Due to their epsilon-near-zero or mu-near-zero behavior and low diffraction nature, they could be the proper candidates for enhancing the transmission. However, both corrugations based and metamaterial based approaches depend on the coupling between the incident waves and propagating surface modes.

CHAPTER 2. THEORETICAL BACKGROUND

To overcome the limitations in the transmission enhancement phenomenon, Aydin et al. and Cakmak et al. designed an SRR coupled metallic screen configuration [38]. Since the dimensions of the SRR are comparable to aperture which is subwavelength, this setup was extremely compact. They achieved 740-fold enhancement with guidance of the incident beam through the subwavelength aperture. Finally, Cakmak et al. discusses the physical origins of the enhancement by analyzing the surface currents in the vicinity of aperture [39].

Chapter 3

Transmission Enhancement using Connected Split Ring Resonators

In this chapter, we propose an alternative way to increase the transmission and obtain an enhancement. We designed a new type of SRR called Connected Split Ring Resonators (CSRR). We demonstrate the transmission enhancement by experiments and numerical analysis. We also analyze the physical origins of transmission enhancement.

Although previous designs (see [38, 39]) propose high enhancement results, our design surpasses those results. Another difference with the previous studies is the orientation of the resonator: instead of covering the sub-wavelength aperture as shown in Figure 3.1, we inserted the split-ring resonator across the aperture as shown in Figure 3.5.

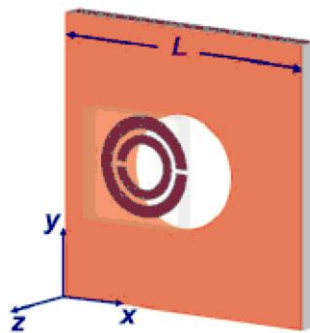


Figure 3.1: SRR coupled subwavelength aperture in the metallic screen design introduced by Aydin et al. [38]

3.1 CSRR Design and Experimental Environment

At the beginning, we used two configurations as building blocks: rectangular SRRs in Sample A, and circular SRRs in Sample B respectively. (See Figure 3.2) Then, we came up with a design by combining two conventional split-ring resonators facing each other, through metal connecting bars as depicted in Figure 3.3 (a) and (b).

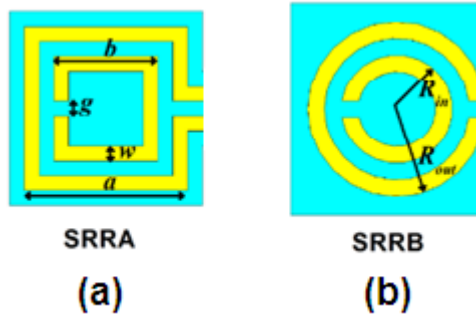


Figure 3.2: Single SRR configurations (a) Rectangular SRR, SRR A and (b) Circular SRR, SRR B.

The SRR samples are deposited on one side of a dielectric printed circuit board (PCB) which is used as the substrate material for these SRR samples. The PCB thickness is 1.6 mm which is deposited with a 30 μm copper. The design parameters are the following: split width $g = 0.5$ mm, which is the same for inner and outer ring (Figure 3.3 (a)), copper width $w = 0.5$ mm, and the separation distance (length of the connecting bars) $l = 5.5$ mm for both SRR configurations, $R_{out} = 3$ mm, and $R_{in} = 1.75$ mm. So, we obtained an opposed pair of SRRs with connecting arms and we named our structures Connected-SRR (CSRR).

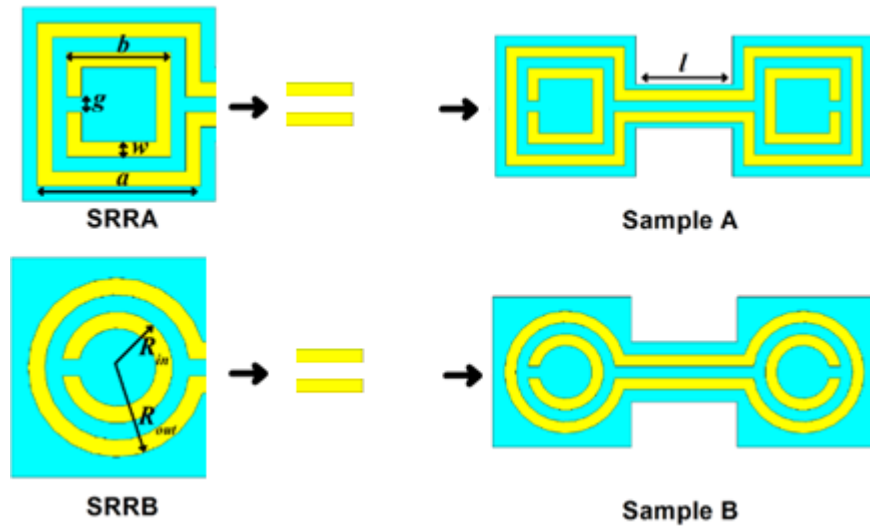


Figure 3.3: SRR and SRRB samples in order to design CSRR samples: Sample A and Sample B

We first simulated the SRR and CSRR designs that are shown in Figure 3.2 and Figure 3.3 to characterize their transmission behavior and adjust the magnetic resonance frequency by changing the dimensions of the structures. We performed several simulations with these SRR and CSRR designs by using CST Microwave Studio. In order to determine the resonance frequencies, we applied periodic boundary conditions and plane wave excitation where the electric field (E-Field component) is parallel to the CSRR splits and magnetic field (H-Field) is perpendicular to the plane of CSRRs.

We obtained resonance frequencies for Rectangular CSRR (Sample A) at 3.61 GHz, Single Rectangular SRR (Single Sample A) at 3.53 GHz, Circular CSRR (Sample B) at 4.34 GHz, and lastly, Single Circular SRR (Single Sample B) at 4.26 GHz which are all between the ranges of interest (3-6 GHz). The transmission spectra are shown in Figure 3.4.

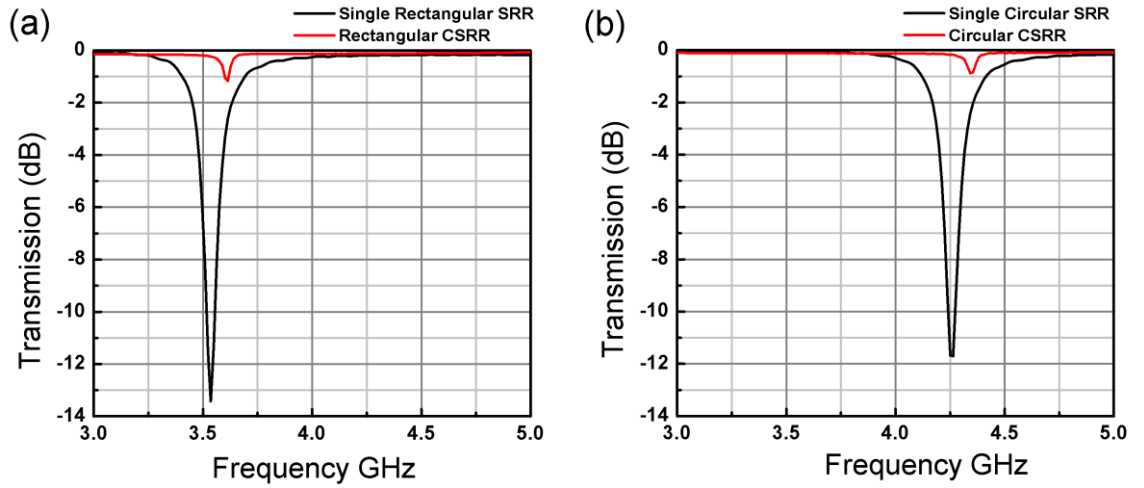


Figure 3.4: Simulated Transmission spectra of (a) SRRB and Sample A, (b) SRRB and Sample B.

In addition to designing the CSRRs, we designed the metallic plate that will be used for large screen during the experiments. The metallic screen is a 50 cm x 50 cm copper plate with a thickness of 0.5 mm. The metallic screen was chosen as large as possible to reduce the effects of the diffraction from the edges. In the middle of the plate, we drilled a rectangular aperture with a width of 3 mm and height of 7.5 mm. This aperture size is smaller than the other reported aperture sizes in literature. [38, 39]. (See Figure 3.5)

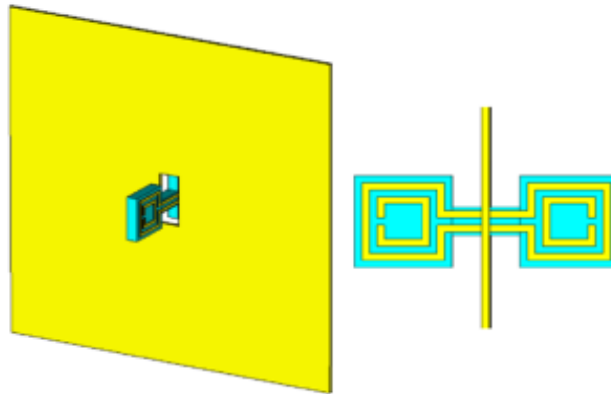


Figure 3.5: Sample A incorporated in the aperture.

Next we started our experiments. During the experiments, we used conventional waveguide antennas with the operating frequency between 3-6 GHz. These antennas were connected to an HP8510C Network Analyzer as shown in Figure 3.6. The distance between the transmitter and receiver antennas is 8 cm. The transmitter antenna is placed 0.2 mm away from the copper plate to reduce the diffraction effects, since diffraction from the edges of antennas are highly observable.

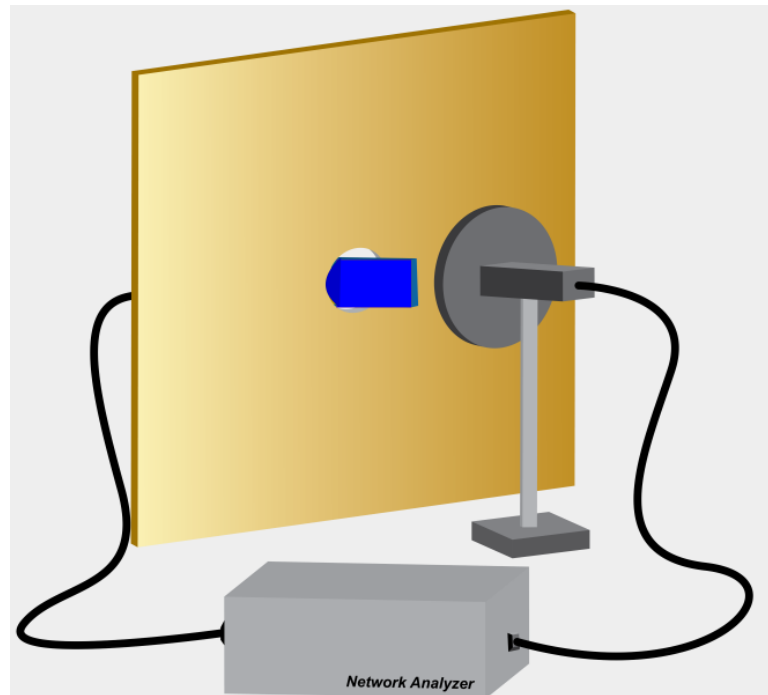


Figure 3.6: Design of the experimental setup.

3.2 Measurement and Simulation Results

At the first stage, we calibrated the network analyzer and measured the background noise without metallic plate and CSRR samples. We placed electrically large Copper plate without inserting the CSRR between the transmitter and receiver, with the distance given in the previous section.

Then we performed our first actual measurement by using the metallic plate that has a single aperture without inserting CSRR. We performed the next measurement by inserting Sample A across the rectangular aperture which is perpendicular to the plane of the metallic plate. At the final stage, similarly, we performed the third measurement by inserting the Sample B into the rectangular aperture. We compared the differences between these three cases.

The “enhancement factor” is calculated by dividing the linear transmission values of CSRR incorporated with metallic plate to the linear transmission values of metallic plate without CSRR, for every frequency point within the bandwidth of interest.

$$\text{Enhancement factor} = \frac{|S_{21}| \text{ with CSRR}}{|S_{21}| \text{ without CSRR}} \quad (1)$$

The measured transmission results are depicted in Figure 3.7 and enhancement results are depicted in Figure 3.8. According to Figure 3.7, we observed that a single peak occurs at a particular frequency for the case of CSRR incorporated with metallic plate. The peak is the evidence of the transmission enhancement phenomenon. The experimental setup and the fabricated structure are also shown in Figure 3.9.

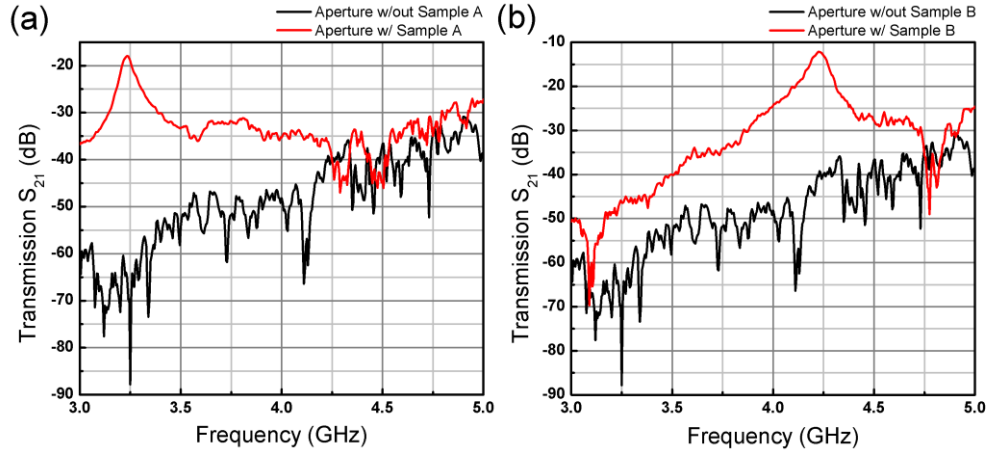


Figure 3.7: Measured Transmitted Intensity through
(a) Sample A (solid red line) and Single Aperture (solid black line) and
(b) Sample B (solid red line) and Single Aperture (solid black line).

The enhancement results are shown in Figure 3.8 (a) and (b) with CSRR Sample A and CSRR Sample B. For the case of Sample A; we observed more than 70,000-fold enhancement factor at 3.23 GHz whereas for sample B, we obtained more than 5,300-fold enhancement at 4.03 GHz through the subwavelength aperture with a width of $\lambda/31$ and a height of $\lambda/12$. These results are much higher than the previous reported results in the literature.

CHAPTER 3. TRANSMISSION ENHANCEMENT USING CSRRS

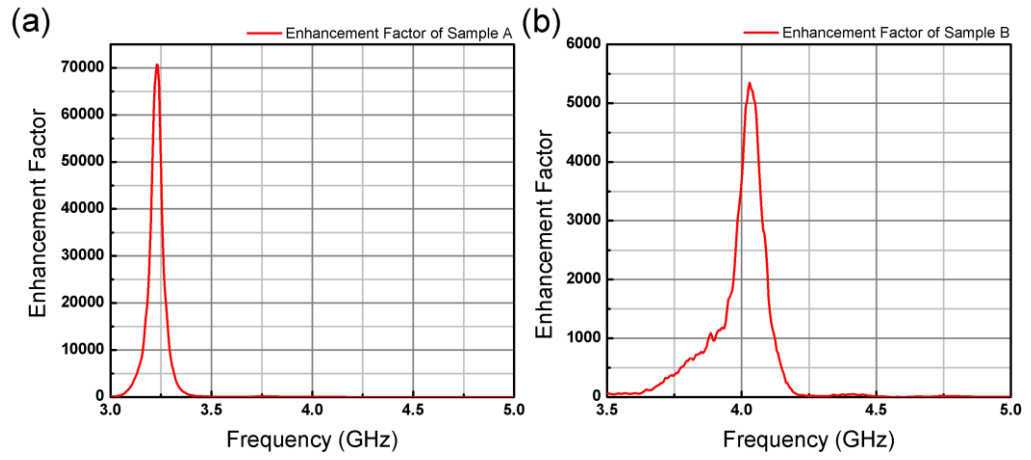


Figure 3.8: Calculated Enhancement Factors from measurement results for (a) Sample A and (b) Sample B.

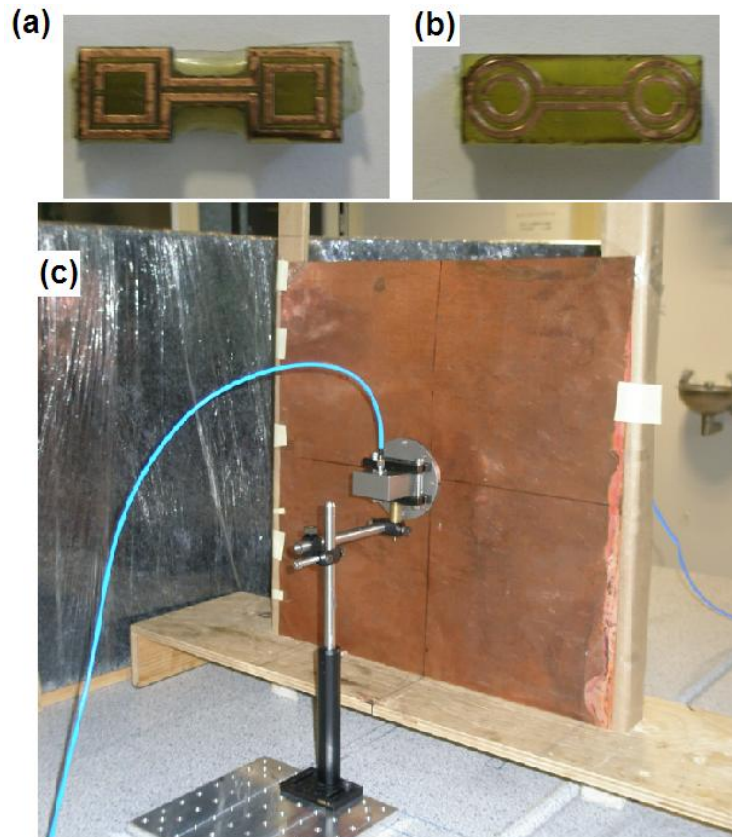


Figure 3.9: Fabricated Samples (a) Sample A, (b) Sample B and (c) Experimental setup.

CHAPTER 3. TRANSMISSION ENHANCEMENT USING CSRRS

After the successful experiments; we simulated the experimental environment once more by using CST Microwave Studio. We adopted the conventional waveguide antenna from the experiments and designed them by being loyal to the same dimensions. We employed open boundary conditions in all directions. Also, we designed PCB with dielectric constant $\epsilon = 4$ and a loss tangent $\delta = 0.01$. We have used lossy copper for the metal plate.

As shown in Figure 3.10 the simulation results match with the experiment results. We achieved to show that the enhancement peaks in the simulations and the actual experimental results are very similar. There is a minor shift in the peaks due to alignment of the antennas and CSRR in the aperture during the experiments, as well as fabrication issues of the CSRRs and metallic plates.

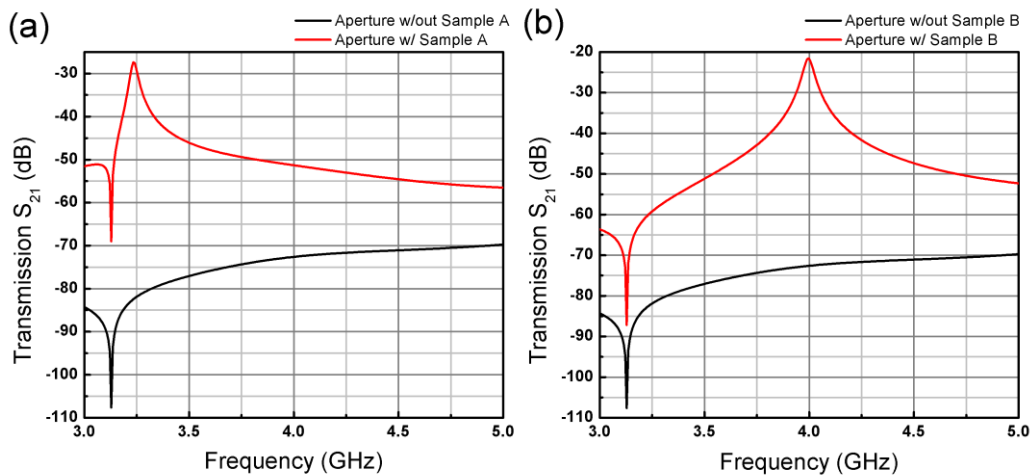


Figure 3.10: Simulated Transmission Intensity Spectra for (a) Sample A (solid red line) and Single Aperture (solid black line), (b) Sample B (solid red line) and Single Aperture (solid black line)

3.3 Physical Analysis and Observations

In this section, we analyze the transmission enhancement from different aspects and discuss the reasons why enhancement occurs.

The primary reason of transmission enhancement is the magnetic resonance of the SRRs. The electric fields in the loops of SRRs are coupled with each other. For our CSRR structure, the field is coupled within the loops and localized. Consequently, the incoming waves are guided from the incident side of the CSRR through the aperture to the exit side of the CSRR.

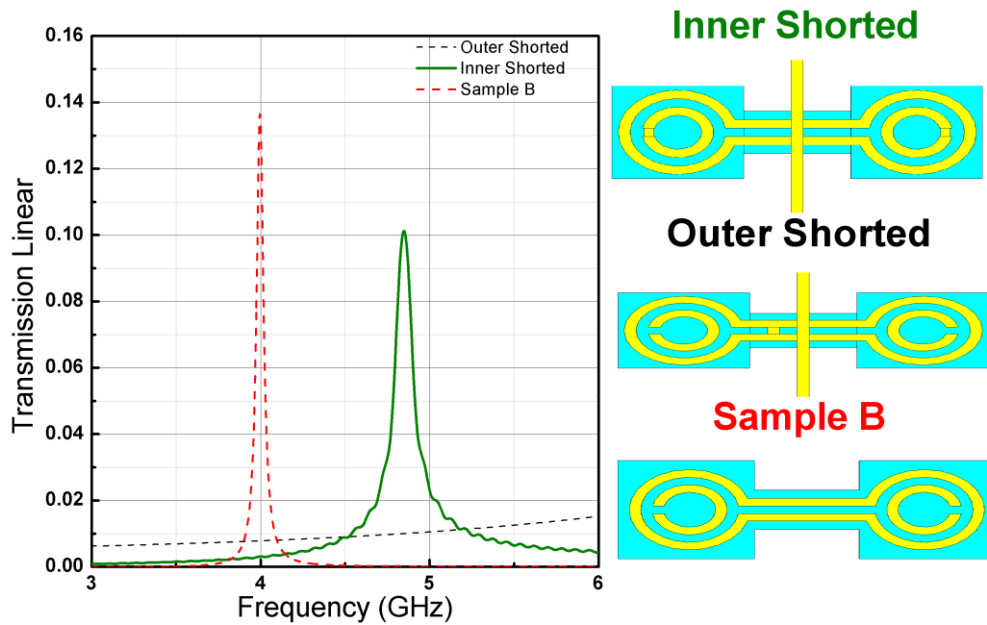


Figure 3.11: Simulated Transmitted Electric Fields Results corresponding to transmission through Single Aperture incorporated with Sample B (dashed red line), Inner Rings shorted Sample B (solid green line), and Outer Rings shorted Sample B (dashed black line).

Here, we investigate the role of magnetic resonance when the loops of CSRRs are shorted. We aim to destroy the magnetic resonance when we short the loops of the CSRRs. Again, we used CST Microwave Studio simulation tool and employed periodic boundary conditions as well as applying plane wave excitation. For this case we have chosen CSRR Sample B to analyze this effect. As Fig-

CHAPTER 3. TRANSMISSION ENHANCEMENT USING CSRRS

Figure 3.11 represents the simulation results of the shorted and non-shorter CSRRs, shorting the outer rings destroys the magnetic resonance at 4.00 GHz whereas, shorting the inner rings only shifts the resonance frequency to higher frequencies. Hence, shorting the inner rings does not affect the existence of magnetic resonance at all. Since the outer ring still keeps its loop geometry, it dominates the magnetic resonance. Therefore, the outer ring is still responsible for the transmission enhancement.

From a different point of view, we investigated the effects of the aperture size on the CSRR-aperture system. This study has been analyzed previously by Cakmak et al. [39]. In this previous study, the authors analyzed the effects of changing the aperture size on subwavelength transmission enhancement (STE) factors and frequency. In this paper, STE factor is defined as the multiplication of transmission enhancement with (R/λ) where R is the aperture radius and λ is the operational wavelength.

$$\text{STE factor} = \text{Enhancement factor} * \frac{R}{\lambda} \quad (2)$$

In that study, the resonator sizes were comparable to the subwavelength aperture size. The aperture radius ranged from 2.4 mm to 7 mm. They observed that the resonance frequency decreased as the radius of the aperture increased. Also, they found that the optimal aperture geometry has a radius of around 4.8 mm by using the STE factors. (See Figure 3.12) Finally, they concluded that any change in the geometry or size of the aperture could affect the resonance frequency.

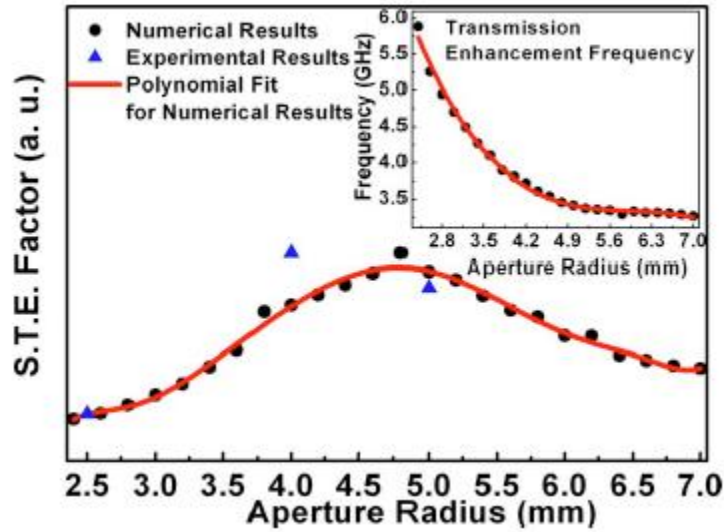


Figure 3.12: STE factor for various radii in the range 2.4-7 mm where the black dots are the numerical results and red line is experiment organized by Cakmak et al. [39]

However in this study, we designed a resonator such that the resonance frequency is more stable with respect to the changes in aperture size and geometry. Our design consists of two copper plates each having a single aperture: Aperture 1 (Copper plate 1) and Aperture 2 (Copper plate 2). Aperture 1 has dimensions 1 mm x 2.5 mm whereas Aperture 2 has dimensions 3 mm x 7.5 mm width and height respectively.

We designed another resonator with outer loop ring lengths 12.5 mm and inner loop lengths 10.5 mm. This new resonator is slightly larger than the previous CSRR. Figure 3.13 shows the apertures and this resonator. We simulated them by applying periodic boundary conditions and plane wave excitation. The measured transmission spectrum is shown in Figure 3.13. We observed similar amounts of enhancement factors at the same frequency when we use circular and rectangular apertures with the same large CSRR. Thus, the transmission frequency is independent of the aperture size, only the enhancement factor magnitude changes.

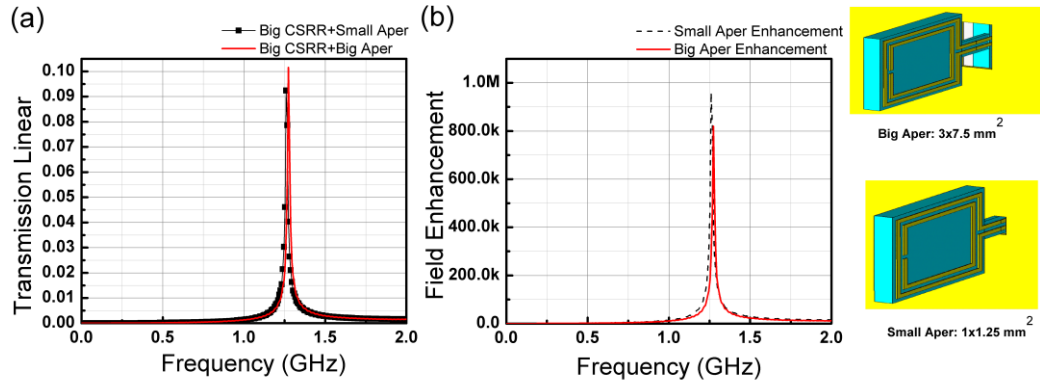


Figure 3.13: (a) Simulated transmitted electric field through Big CSRR in the small aperture (black line) and Big CSRR in the big aperture (red line), (b) Simulated Field Enhancement of Big CSRR through the small aperture (black line) and the big aperture (red line)

As a final remark, we discuss the effect connecting bars on transmission enhancement. In previous studies, researchers obtained enhancement by covering half of the aperture without having connecting bars [38, 39]. We used the similar design but instead of placing the SRR parallel to the plane of plate; we placed it perpendicular to the plane of plate. We also omitted the exit side of the CSRR Sample A. Single SRRs caused relatively smaller enhancement than factors the other CSRR cases. In [38] and [39], the researchers obtained a 740-fold enhancement factor. However, in our case with CSRR, we achieved more than 70,000-fold enhancement.

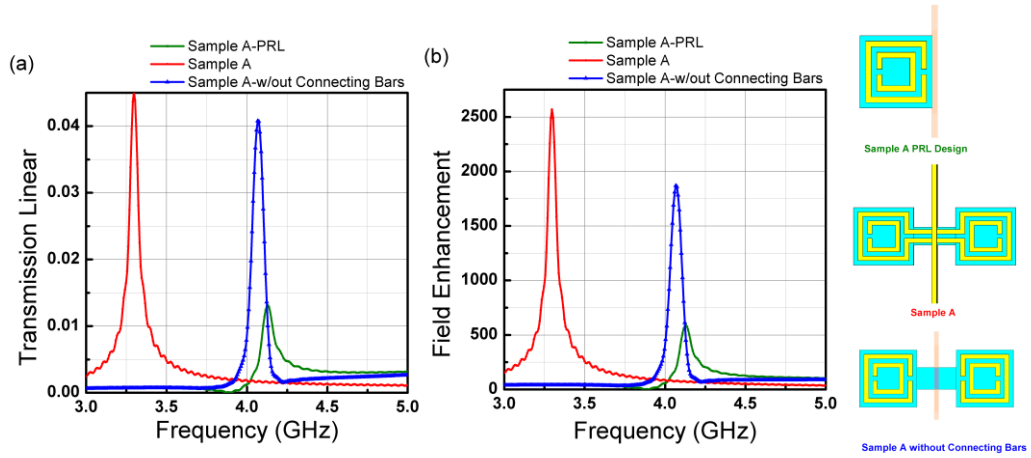


Figure 3.14: (a) Simulated transmitted electric field of Sample A (red line), Sample A PRL design (green line) and Sample A without Connecting bars (b) Simulated Field enhancement of of Sample A (red line), Sample A PRL design (green line) and Sample A without connecting bars

Next, we simulated the CSRR without connecting bars. This structure has two SRRs but no connecting bars. We simulated this structure and analyzed both with CSRR Sample A, CSRR Sample A without connecting bars and single SRR as shown in Figure 3.14. We observe that CSRR Sample A and CSRR Sample A without connecting bars still have similar amount of enhancements with a slight frequency shift. On the other hand; single SRR has a relatively small enhancement. CSRRs without connecting bar have a better coupling than Single SRR due to exit side SRR. Also, due connecting bars, the CSRR inserted in the aperture system has a frequency independency from the aperture increasing and has an increased coupling.

Furthermore, we analyzed the electric fields through the CSRRs, the connecting bars, the aperture and CSRRs without connecting bars. As shown in Figure 3.15 (a) the surface currents are distributed equally on both the input and output side of CSRR, which is the evidence of coupling between input and output sides. Figure 3.15 (b) demonstrates the highly localized electric fields around the aperture due to CSRRs. On the other hand, the second SRR is also highly coupled without connecting bars (Figure 3.15(c)). Single SRR might be useful to

have more E-Fields, however it poorly guides the E-Fields to the exit side SRR. Both input and output SRRs behave like transmitter and receiver antennas. We observed from Figure 3.15 (d) that the incoming fields are localized around the aperture and guided to the exit side SRR successfully via connecting bars. The exit side SRR is highly excited with the aid of these connecting bars.

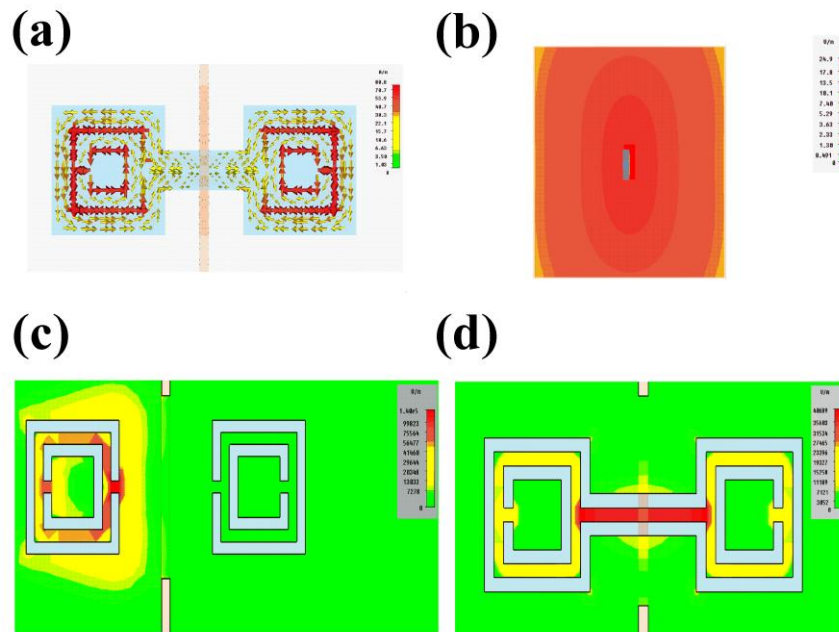


Figure 3.15: (a) Induced surface currents when the CSRR is excited, (b) Field localization around the aperture, Electric field localization in the vicinity of the aperture when the CSRR exists (c) without connecting bars, (d) with connecting bars.

As a conclusion, in this section, we presented an alternative approach that offers higher transmission enhancement results than the other reported ones. We first numerically characterized the CSRR configurations. Then, we obtained the transmission enhancement results experimentally. We verified them with the simulations once more by applying the experimental environment in the simulations. We achieved more than 70,000-fold enhancement at the single frequency as anticipated through subwavelength apertures ($\lambda/31$ width x $\lambda/12$ height). We

CHAPTER 3. TRANSMISSION ENHANCEMENT USING CSRRS

finally analyzed the mechanism that generate or dominate the resonance frequency.

Chapter 4

Transmission Enhancement using Omega-like Split Ring Resonators

The Omega-like particles were first introduced by Saadoun and Engheta in 1992 [40]. The authors showed these particles have *bi-anisotropic* and *pseudo-chiral* effects, so they are artificial materials. The omega particles were then analyzed by other physicists such as Tretyakov, Simovski and Sochova [41]. Omega particles were demonstrated as a successful candidate for left-handed metamaterials [42]. By using omega-like metamaterials, the intrinsic chirality of the medium can be eliminated and a moderate bandwidth can be obtained [43, 44]. To realize these characteristics, two omega-like resonators should be placed on opposing sides of a printed circuit board in opposite directions as shown in Figure 4.1 (a).

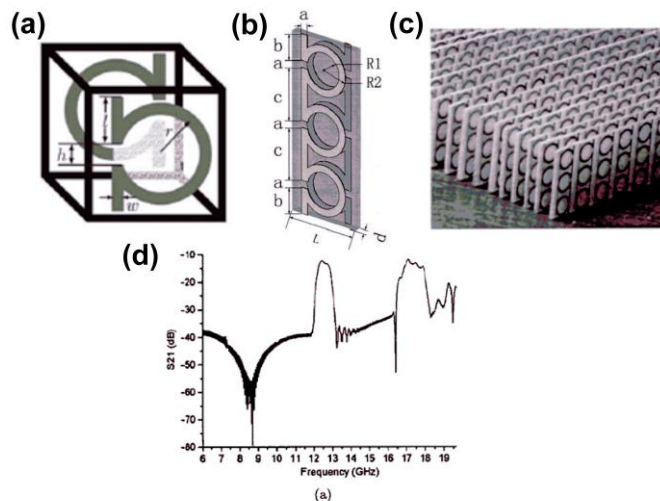


Figure 4.1: Omega samples when (a) deposited both sides, (b) an array that includes three Omega Samples, (c) a periodic array in both sides, (d) example of a transmission spectrum.

Also, Aydin et al. experimentally and numerically demonstrated omega inclusions as a type of SRR and analyzed their characteristics [44].

There are some advantages to using Omega-like SRRs such as they are *low-loss* and *pseudo-chiral*. Using these Omega designs in transmission enhancement experiments, we can obtain even higher enhancement factors than those demonstrated in Chapter 3.

4.1 Omega-like Split Ring Resonator designs

Previously, we connected two conventional SRRs with connecting bars to use them for guidance and to obtain a better coupling at the output side of the metallic screen. In this case, similarly, we aim to use two omega-like SRRs to guide and couple the electric fields even more.

In this study, two omega-like SRRs as shown in Figure 4.1 are connected through their arms as shown in Figure 4.2 (a). We fabricated these samples by printing two identical particles (SRRs) in opposite directions on the two sides of a printed circuit board (PCB). The thickness of PCB (FR-4 dielectric board) is 0.5 mm with a 35 μ m copper deposition which can be seen in Figure 4.2 (a) and (b). In the previous case, CSRR was deposited and etched only one side of the PCB; in this case, we deposited and etched the Omega samples on both sides of the PCB.

The geometrical parameters of these Omega-like SRRs are as follows: the radii of the loops are $r = 3$ mm, the width of the metal is $w = 1$ mm, the height of the PCB is $h = 7.5$ mm, single arm length $l = 4$ mm. (see Figure 4.2 (a) and (b))

We also designed the large copper plates that will be used in the experiments with dimensions 700 mm x 700 mm with a thickness of 0.5 mm. The first metallic plate (Plate 1) has a circular aperture in the middle of the plate with a radius of 3.75 mm whereas the second plate (Plate 2) has a rectangular aperture with dimensions 3 mm x 7.5 mm width and height respectively as shown in Figure 4.2 (c) and (d). The heights of the apertures are the same as the heights of the Omega-like SRR in order to cover the aperture vertically.

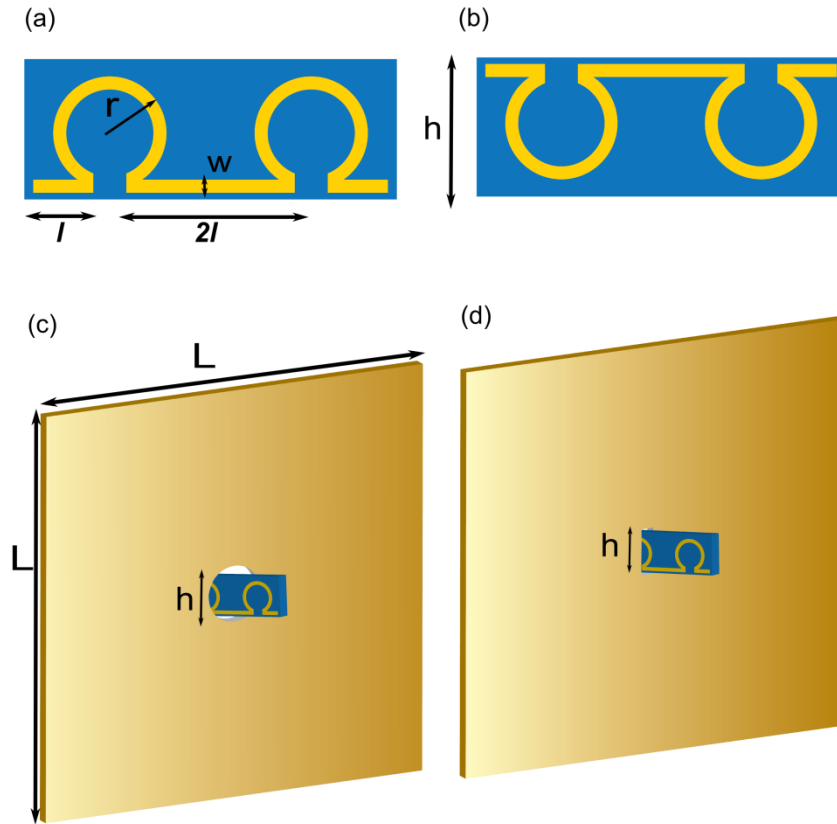


Figure 4.2: a) Schematic of the designed omega-like split-ring resonators from the front side where the parameters are $r = 3$ mm, $w = 1$ mm, and $l = 4$ mm.
 (b) Designed omega-like split ring resonator from the back side.
 (c) Copper screen with omega-like split-ring resonators inserted in the circular aperture where the dimensions are $h = 7.5$ mm and $L = 700$ mm.
 (d) Copper screen with omega-like split-ring resonators inserted in the rectangular aperture

4.2 Experimental Environment

During the experiments, we used metallic plate 1, plate 2 and Omega-like SRRs. The Omega samples were inserted across the apertures specified in the previous section.

We performed the experiments by using conventional waveguide antennas operating within the frequency range 3-6 GHz. The metallic plates incorporated with Omega samples are placed one by one between these antennas which were

connected to an HP8510C Network Analyzer as depicted in Figure 4.3. Then, we collected the S21 data of each metal plate with and without Omega samples.

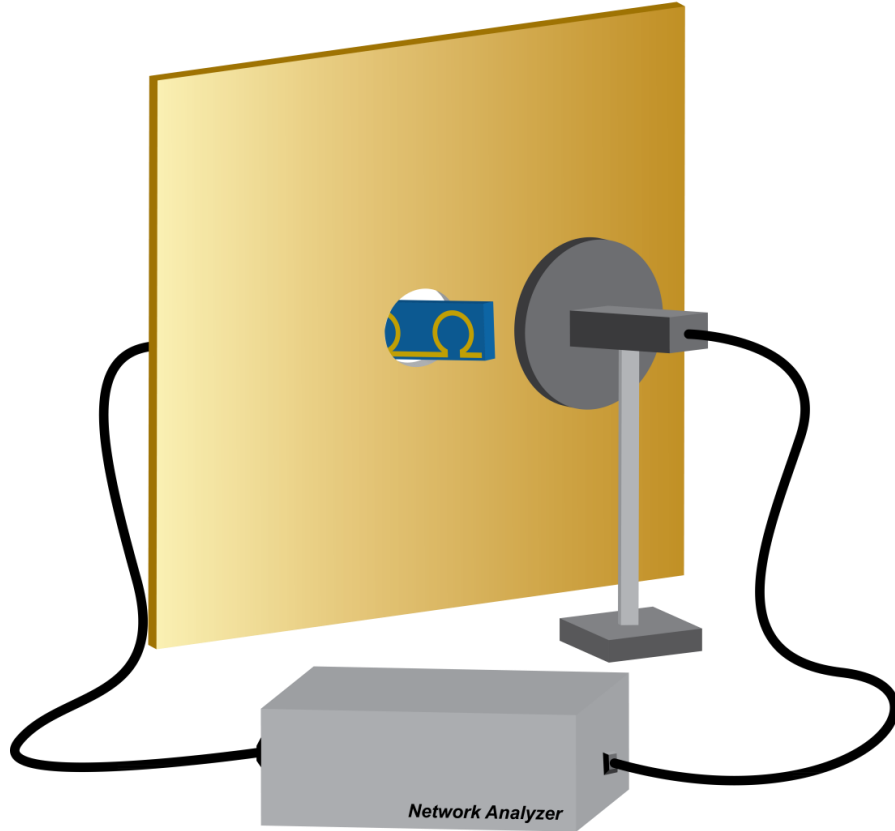


Figure 4.3: Schematic demonstration of the transmission enhancement experiments using waveguide antennas and HP8510C network analyzer.

4.3 Transmission Enhancement Results

We performed our first measurement with the copper screen having a circular aperture after calibrating the network analyzer with antennas. The distance between the transmitter and receiver antennas is 8 cm. The transmitter antenna is 0.2 mm away from the metal screen.

Next, using the same plate with circular aperture, we inserted the Omega-like SRR across the aperture and performed the second measurement. The results are shown in Figure 4.4 (a). After obtaining the two S21 parameters, we calculated the enhancement results regarding these S21 values. The enhancement is calcu-

lated as the ratio of linearized S21 values of two cases for every frequency point between the ranges of interest. These calculations are for metallic plate with a circular aperture; then we applied the same procedures for the case of metallic plate with a rectangular aperture. Similarly, we obtained two transmission result and we calculated the enhancement factor for metallic plate with a rectangular aperture. The transmission measurement results are shown in Figure 4.4(b).

According to these results, we obtained two enhancement peaks for both cases as presented in Figure 4.5. In both cases, the first peak is at 3.15 GHz and the second peak is at 3.95 GHz. Through circular aperture, we obtained 4,014-fold enhancement at the first peak (3.15 GHz) and 9,262-fold enhancement at the second peak (3.95 GHz). For the case of rectangular aperture, we achieved a 20,780-fold enhancement at the first peak and 154,500-fold enhancement at the second peak. As we expected; these results are the highest results in the literature [38, 39, 45, 46].

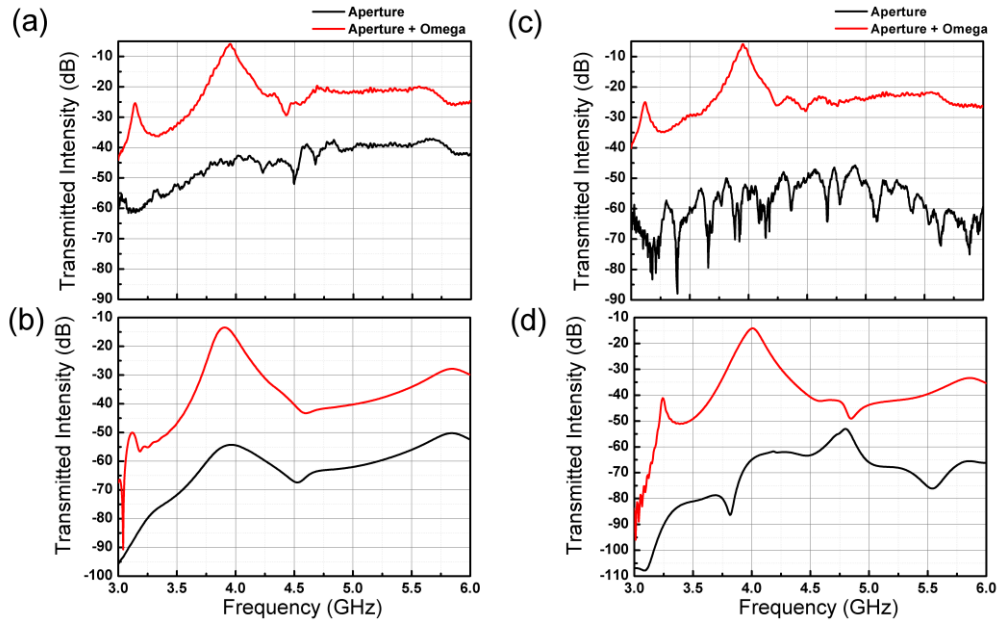


Figure 4.4: (a) Experimental and (b) simulation results of the transmission intensity (dB) through the circular aperture (c) experimental and (d) simulation results for the rectangular aperture (solid black line is for the single aperture, solid red line is for the omega-like split-ring resonators inserted across aperture.)

CHAPTER 4. TRANSMISSION ENHANCEMENT USING OMEGA-LIKE SRRS

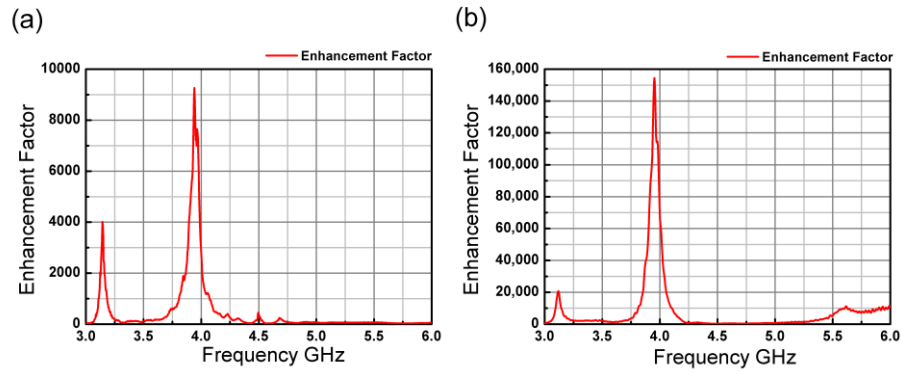


Figure 4.5: Enhancement factor in the case of the omega-like split-ring resonators inserted (a) across the circular aperture and (b) across the rectangular aperture.

4.4 Verification of Experiments through Simulations

To validate the experiments, we numerically analyzed the system by using CST Microwave Studio. Initially, we modeled the two conventional waveguide antennas. We excited the antennas via waveguide ports. Open boundary conditions were employed for the environment throughout the simulations.

We chose the relative dielectric constant $\epsilon = 4$ and a loss tangent $\delta = 0.01$ while modeling FR 4 PCB. The simulation results are shown in Figure 4.4 (c) and (d). As anticipated, the simulations provided better transmission results and higher enhancement factors due to various reasons such as diffractions at the edges of metallic screen which are cut off in simulations. Also, the dimensions of the samples are not exactly the same as the ones in the simulations due to manufacturing constrains.

4.5 Physical Analysis of Transmission Enhancement via Omega-like SRRs

We obtained two enhancement peaks in the experiments. In this subsection, we discuss why these peaks occur by giving geometrical and electromagnetic explanations.

As any symmetric structure in nature supports two fundamental modes of operation, our Omega SRR - Aperture system has these modes. One of these two modes is characterized by an even field symmetry which is evenly distributed electric field on the two halves of the structure with respect to the plane of metal plate. The other is the odd field symmetry that the electric field is oddly distributed.

The loops of the Omega-like SRRs act like an electrically short antenna working one in the transmitting mode on the one side of the plate; another in the receiving mode on the other side of the plate.

Additionally, we state that at the frequency for which the electric field exhibits an even symmetry, the arms of Omega samples are not excited. However, the two

CHAPTER 4. TRANSMISSION ENHANCEMENT USING OMEGA-LIKE SRRS

antennas are electromagnetically coupled through the aperture. Figure 4.6 (a) shows that at the first enhancement peak (3.15 GHz) strong coupling occurs but not through arms with the aid of surface currents.

Conversely; at the frequency for which the electric field exhibits an odd symmetry, the arms of Omega samples are strongly excited. As we can see from Figure 4.6 (b), the structure is simulated at the second enhancement peak (3.95 GHz). The figure presents that the two antennas provide higher transmission as they are connected by a transmission line leading a strong coupling. Hence, we can deduce that the first peak originates from an even mode, whereas the second one from the odd mode. For further information about the behavior at the non-resonant frequencies, we simulated the surface currents at 5.00 GHz which is after the two resonant peaks in the spectrum. (See Figure 4.6 (c)) This implies that the two antennas (meaning Omega at the one side and the other) are not coupled at all and we cannot observe any transmission enhancement.

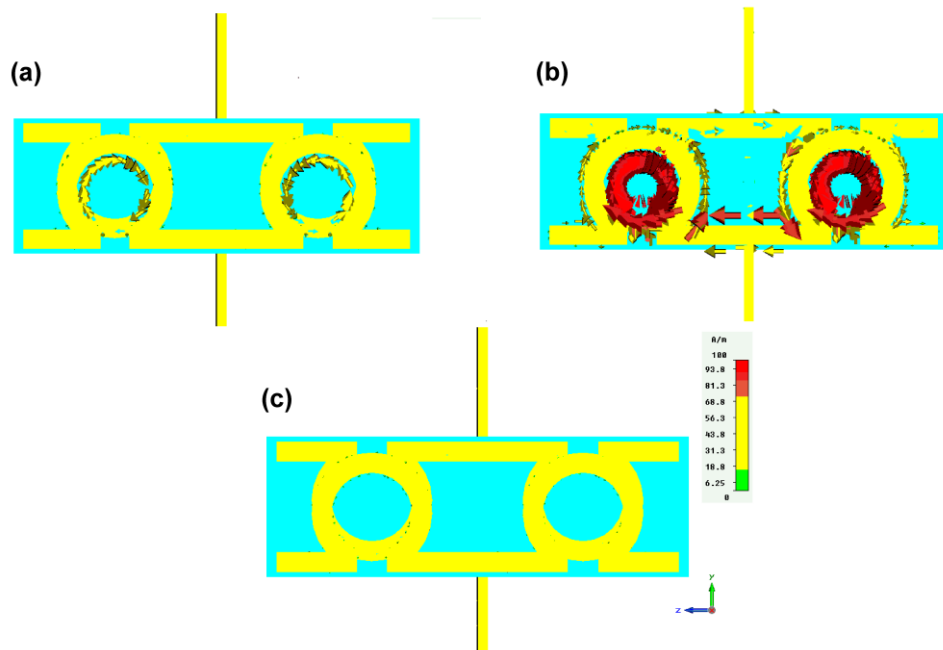


Figure 4.6 Surface current density (a) at 3.15 GHz (even mode operation) where the first enhancement peak occurs, (b) at 3.95 GHz (odd mode operation) where second enhancement peak occurs, (c) at 5.00 GHz (non-resonant frequency) where no enhancement occurs.

4.6 Parametrical Analysis that Strengthen the Physical Observations

In section, we would like to understand the effects of circular, rectangular apertures and various Omega configurations.

We showed the aperture independency of the enhancement frequency in Section 3.3. Here, we still expect the enhancement peaks to be independent from the size and geometry of the apertures. The size and geometry of the apertures only influence the transmission intensity and the enhancement factors. Due to lower aperture area, when using the rectangular aperture instead of the circular one, the transmission intensity is expected to be lower, thus when inserting the omega shaped split-ring resonator, the enhancement factor is expected to be higher. The transmission difference between the circular and rectangular apertures is depicted in Figure 4.7 (a). According to this graph, a circular aperture has higher transmission intensity due to geometry. The calculated enhancement factor difference is shown in Figure 4.7 (b). As explained, by using a rectangular aperture we can obtain 154,500-fold enhancement.

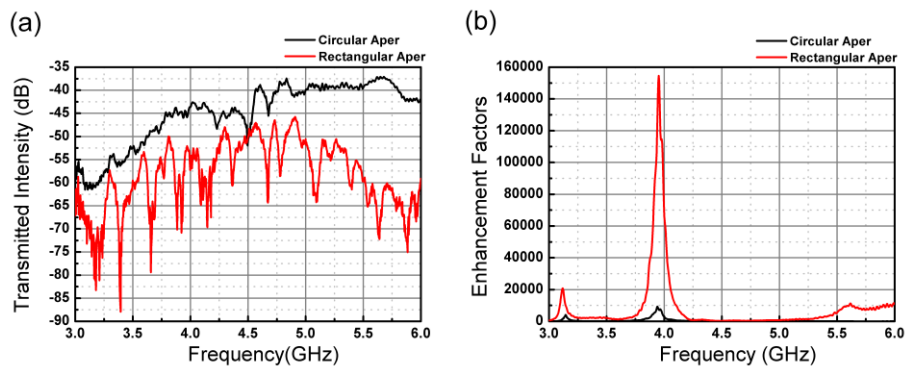


Figure 4.7 (a) Difference of the transmission through circular and rectangular apertures and (b) difference of the enhancement factor when omega-like split-ring resonators are inserted across circular and rectangular apertures.

CHAPTER 4. TRANSMISSION ENHANCEMENT USING OMEGA-LIKE SRRS

We have also analyzed the effects of the double-sided deposited and single-sided deposited omega-like SRRs. In the first case, we considered the samples that are produced by two identical Omega-like SRR samples printed in opposite directions on the two sides of the FR-4 board (PCB) which is named as “double-sided Omega-like SRRs”. The samples which are named as “single-sided” are produced by single Omega-like SRR printed on one of the sides of the PCB. Here, we propose the reason of the enhancement is due to the symmetric design of the Omega-like SRRs. In order to demonstrate the effect of the symmetric and non-symmetric design, we have analyzed the electric field distribution maps for three different cases that are shown in Figure 4.8. These cases are the field distributions of the double-sided Omega-like SRRs inserted in the rectangular aperture (Figure 4.8 (a)), single-sided Omega-like SRR inserted in the rectangular aperture (Figure 4.8 (b)) and rectangular aperture without Omega-like SRRs (Figure 4.8 (c)) at the frequencies 3.95 GHz (highly resonant frequency where second enhancement peak occurs) and 5.00 GHz (non-resonant frequency where no enhancement occurs).

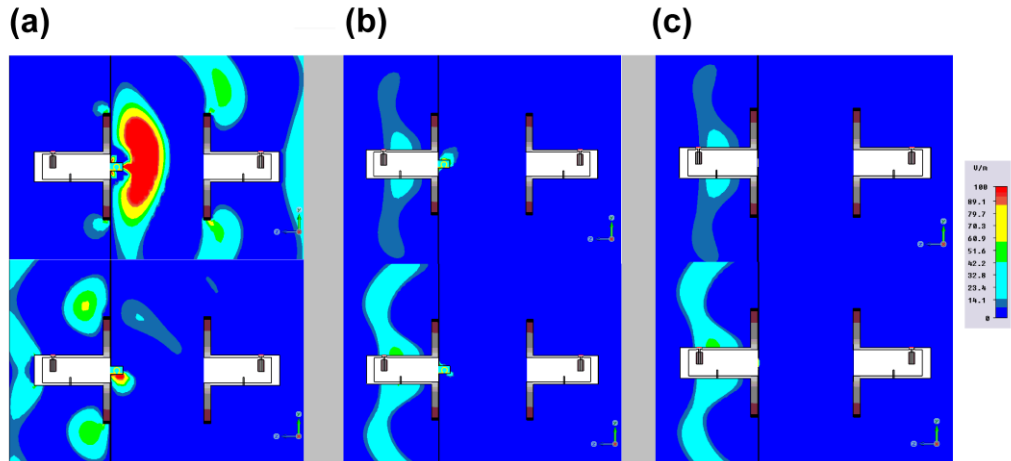


Figure 4.8: Electric Field Distribution maps of the (a) Double-sided Omega-like SRR across the rectangular aperture at 3.95 GHz (above), 5.00GHz (below), (b) Single-sided Omega-like SRR across the rectangular aperture at 3.95 GHz (above), 5.00GHz (below), (c) Rectangular Aperture without Omega-like SRR at 3.95 GHz (above), 5.00GHz (below).

In Figure 4.8 (a), we observed that the electric field distribution is strong at the resonant frequency (above) and weak at the non-resonant frequency (below).

CHAPTER 4. TRANSMISSION ENHANCEMENT USING OMEGA-LIKE SRRS

Although the field is simulated at the same resonant frequency in Figure 4.8 (b) (above), the field strength is weak. This weakness occurs due to non-symmetric nature of the Omega-like SRRs design. In other words, the strong enhancement is achieved when the double-sided (symmetric) Omega-like SRRs is used. Finally, the field distributions which represent weak transmission in the absence of Omega-like SRRs are observed in Figure 4.8 (c) at 3.95 GHz (above) and 5.00 GHz (below). In this case, there is low transmission and hence no enhancement can be obtained due to absence of the resonator.

A deeper analysis has been done by comparing the transmission spectra of the double-sided and single-sided Omega-like SRR, and in the absence of it across the rectangular aperture in Figure 4.9 (a). As shown in the figure, when the single-sided Omega-like SRR is used instead of the double-sided one, it is apparent that enhancement peaks vanish and transmission behaves as in the case of the absence of Omega-like SRRs. Furthermore, we obtained the field distribution maps for these three cases by field monitors at the highly resonant frequency (3.95 GHz) as in Figure 4.9 (b), (c), and (d). The strong coupling between the receiver and transmitter compartments occurs due to double-sided Omega-like SRR as shown in Figure 4.9 (b), whereas in Figure 4.9 (c), coupling is destroyed by using single-sided Omega-like SRR. Also, in the absence of Omega-like SRRs, there is no coupling; hence no transmission enhancement occurs as presented in Figure 4.9 (d).

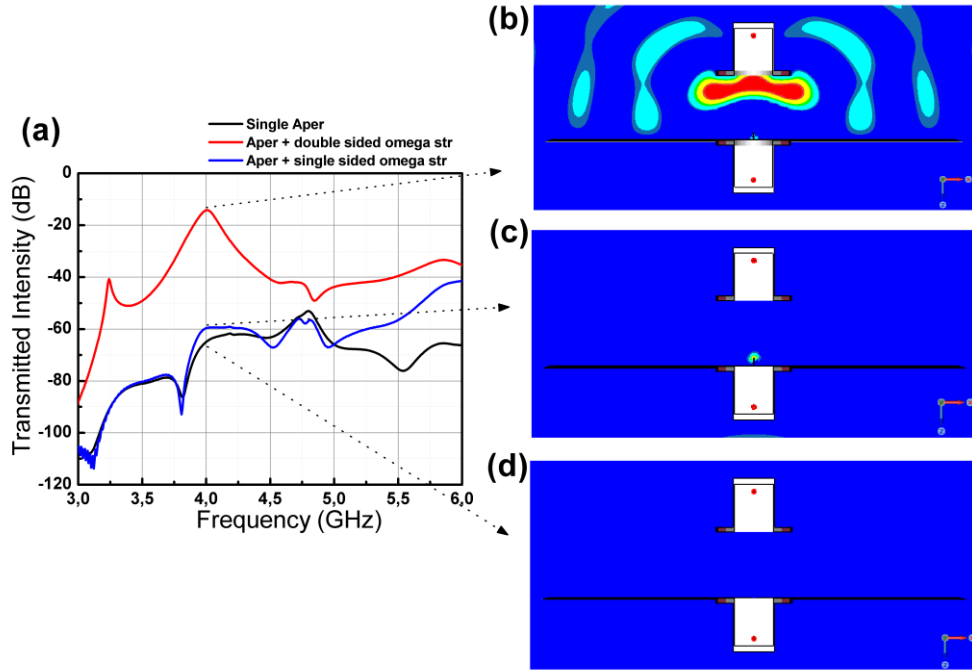


Figure 4.9: (a) Transmission characteristics of Double-sided (Solid Red), Single-sided Omega-like SRRs (Solid Blue), Aperture without Omega-like SRRs (Solid Black), (b), (c) and (d) Electric Field Distribution Maps collected at 3.95 GHz (Resonance Frequency) respectively.

Finally, we analyzed the field localization of the transmitted wave at the exit side of the Omega-like SRRs. In this case, we used double-sided Omega-like SRRs analyzed at the highly resonant frequency (3.95 GHz). The electric fields at the various distances in the direction of the propagation at the exit side of Omega samples are collected by electric field probes. We calculated the normalized electric field intensity by using the data from the probes. The normalized electric field intensity of the transmitted wave versus distance away from the Omega-like SRR in terms of operational wavelength is depicted in Figure 4.10 (d). In the figure, the transmitted wave decays as the electric field probe moves away from the Omega-like SRR at the exit side. Figure 4.10 (a) represents the field distribution when the probe is 0.1λ away from the Omega-like SRR, (b) represents when the probe is 0.5λ away from the Omega-like SRR and finally (c) represents when the probe is 0.7λ away from the Omega-like SRR. This explains the evanescent field is highly localized near the omega-like SRR and as the

probe moves away from the resonator. Evanescent field decays and results in low transmission.

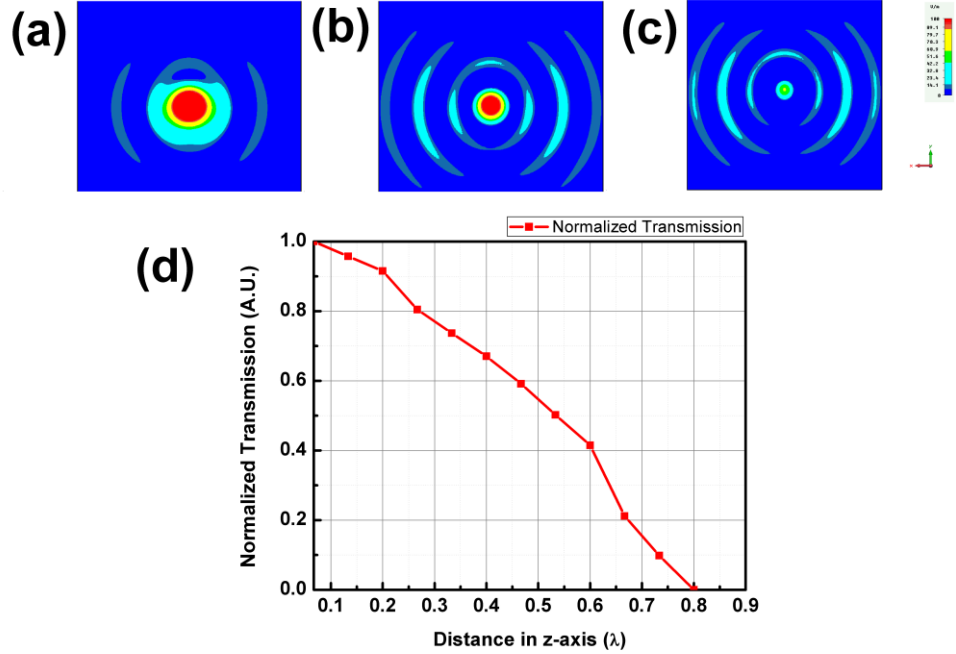


Figure 4.10: Field Distribution Maps (a) 0.1λ away (b) 0.5λ away, (c) 0.7λ away from Omega-like SRR, and (d) Normalized transmitted intensity versus distance away from the Omega-like SRR in terms of operational wavelength.

In this chapter, we presented the transmission enhancement via Omega-like SRR which offers even higher than the previous section. We obtained more than 150,000-fold enhancement experimentally and verified numerically. We also analyzed the effects of the arms, double-sided Omega design, single-sided Omega design and surface currents at the resonant and non-resonant peaks.

Chapter 5

Transmission Enhancement using Stack-like Split Ring Resonators

Until this chapter, we achieved transmission enhancement through subwavelength apertures using various SRR configurations. We first designed CSRR structures in order to reach more than 70,000-fold enhancement. Likewise, after the CSRR designs, we came up with Omega-like SRR designs to pass the previous enhancement factors. By these structures, we could obtain more than 150,000-fold enhancement at a particular frequency.

However, in this case, we desire to obtain a broadband, multi-peak enhancement. As we can realize from the literature, one of the alternative ways to strengthen the band efficiency of the metamaterials is to combine the metamaterial layers one by one as a stack structure [13, 47]. Hence; the single peak or dip can be broaden by stacking the same material arrays one behind another.

Furthermore; the coupled cavity became an attractive topic. The researchers first considered photonic crystals as coupled cavities and obtained band-gaps [48-50]. However, then, the metamaterials were understood that they can be treated as coupled cavities with generating band-gaps [51]. Especially, the composite metamaterials are the good candidates of coupled cavities [51, 52]. Composite metamaterials can be also designed by using SRR arrays. [53].

The stacking idea encouraged us to convert our initial single aperture covered with SRR model to stacked-apertures covered with SRRs model. So, we would achieve a multi-peak enhancement system that is controllable by the geometry of the metamaterials and the distance between the metamaterial arrays (layers). (See Figure 5.1 (a) and (b))

Here; we expect a strong coupling in the system which broadens the enhancement peaks and generates multi-peak resonant transmission spectra. In order to explain the physics behind the enhancement in the transmission spectra, we used Tight Binding (TB) methods. We determined TB parameters and calculate the transmission peaks.

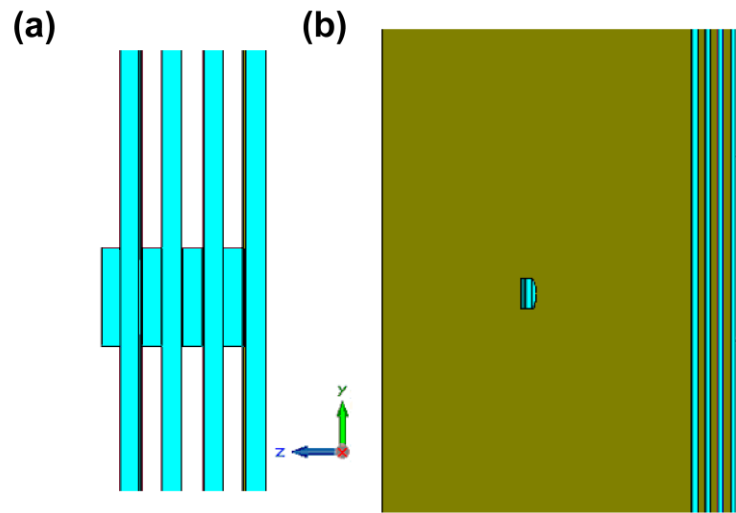


Figure 5.1: Simulation environment of Four Stacked-Four SRR design
(a) from the side, (b) from the front perspective.

5.1 Multi-Stack Design and SRR configuration

Since Aydin and Cakmak et al. designed the first SRR coupled enhanced transmission through subwavelength aperture; the idea has gained more attention. It is not just a coupled system that increases the transmission through subwavelength apertures; but also it adopts the coupled cavity phenomenon [51-53]. They have covered the half of the aperture parallel to plane of plate with a single SRR that has a comparable size to the subwavelength aperture. The SRR is a typical circular SRR as described in [38] and [39].

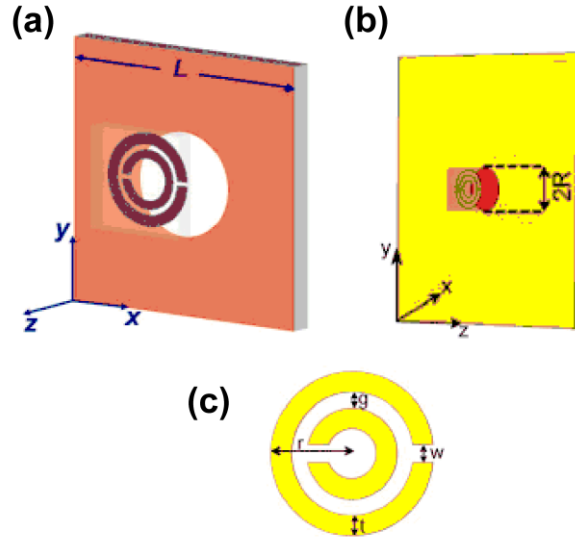


Figure 5.2: (a) and (b) various configurations of SRR coupled single aperture designed by Aydin et al. and Cakmak et al. (c) SRR design from the front view [38, 39].

At the first stage; we adopted the conventional SRR model has been designed by Aydin and Cakmak et al. which has been shown in Figure 5.2. Unlike the SRR inserted across the aperture design in Chapter 3 and Chapter 4, we go back to the initial design which is covering the half of the aperture parallel to the plane of plate. The dimensions of the SRR are $R_{out} = 3.6$ mm, $R_{in} = 2.7$ mm, split between the Copper loops is $s = 0.2$ mm, and width of the loops is $w = 0.9$ mm. The thickness of the deposited copper on the one side of PCB is $30 \mu\text{m}$. Total thickness of the PCB is 1.5 mm with the deposited copper on top of it. The design details are shown in Figure 5.3.

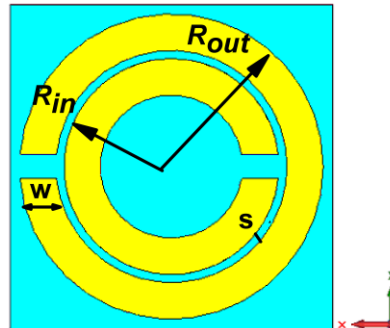


Figure 5.3: SRR design that is used to couple the stacks.

The configuration of the metal screen with a single aperture incorporated with an SRR is shown in Figure 5.4. We used a large PCB with a 290 mm width, a 320 mm height and a 1.5 mm thickness. There is an aperture with a radius of 4 mm in the middle of the PCB screen. To note that, using one side Copper deposited PCB and a Copper metal plate does not affect the transmission measurement since they have the same behavior in the microwave regime. In addition, fabricating properties of PCBs are easier than thick copper plates.

We cover the half of the apertures with the SRRs, the distance between each stack is 1.5 mm. Figure 5.4 (b) and (c) shows the front side and back side configurations of the single stack with single SRR structures. We fabricated four samples of large PCB plates and four SRRs.

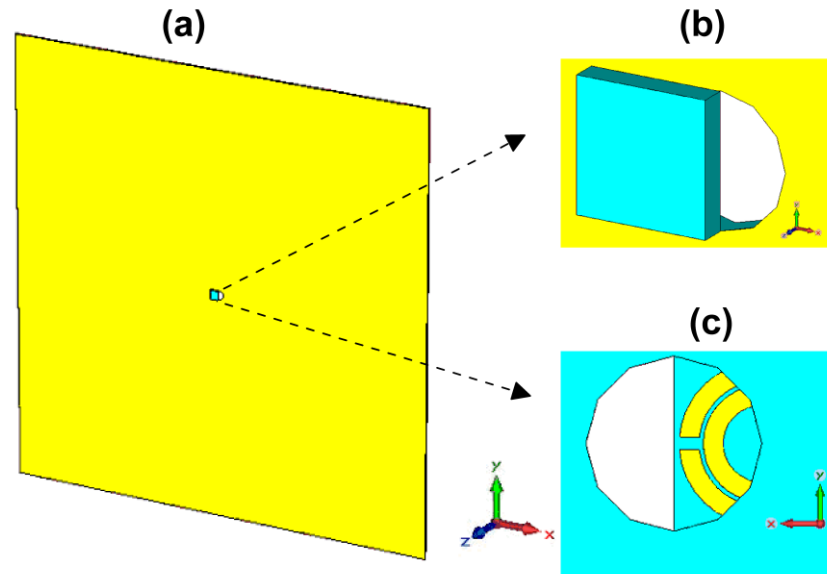


Figure 5.4: (a) SRR cover the half of the aperture, (b) zoomed view from the front side, and (c) zoomed view from the back side.

5.2 Experimental Environment of the Stacked Metal Screens with SRRs and Transmission Spectra

The experimental environment is designed by stacked plates with SRRs, two antennas: one in receiving and the other transmitting mode, and a network analyzer as shown in Figure 5.1 and Figure 5.4. The transmitting antenna is placed as close as possible to the plates in order to reduce the effects of the diffractions. The receiving antenna is placed 3 cm away from the last stack. After we added one more plate behind the last plate, we placed the receiving antenna one period (3 mm) away in order to preserve the 3 cm distance with the last stack. In other words, as we add more stacks, the distance between transmitting and receiving antenna increases.

We began our experiment with the first stack. The first metal plate was located with the SRR that covers the half space of the aperture. The SRR was placed with very thin foam which allows coupling. The conventional waveguide antennas

were connected to HP8510C Network Analyzer. The operating frequency is between 3 GHz and 6 GHz. Then, we collected S21 parameters for each frequency within the range of interest. After the first transmission measurement, we placed the metal plate without SRR, and collected S21 data. As previously described procedure, we calculated the enhancement factors by dividing the linearized S21 data of plate with SRR to plate without SRR. The enhancement factors are shown in Figure 5.5. So, we obtained the enhancement results of the single plate. According to this data, we obtained an enhancement at 3.535 GHz as 300-fold enhancement factor.

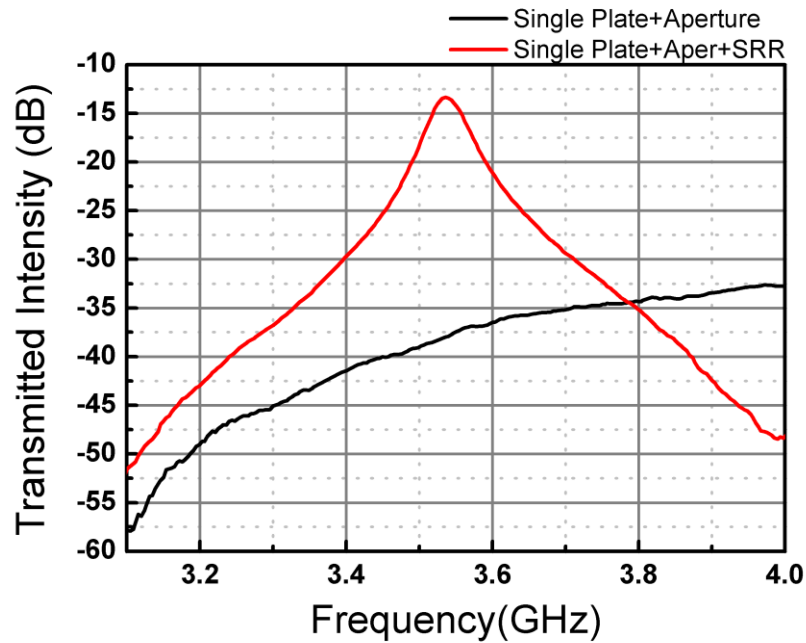


Figure 5.5: Transmission spectra of the SRR incorporated single aperture (red solid line) and single aperture (black solid line).

For the second experiment set, we placed the second metal plate 1.5 mm away from the first plate. We also, shifted the receiving antenna 3 mm away from the previous position. The reason of 3 mm shift is 1.5 mm distance between the stacks and 1.5 mm thickness of the plate. Similarly, we measured the plates with SRRs and the plates without SRRs and applied the same procedures. The enhancement factors of the two-stacked SRR and plate system is shown in Fig-

ure 5.6. Due to double cavity system, we expected two enhancement peaks. According to the results, we obtained two enhancement peaks at 3.357 GHz and 3.632 GHz on the order of 720-fold enhancement and 1070-fold enhancement.

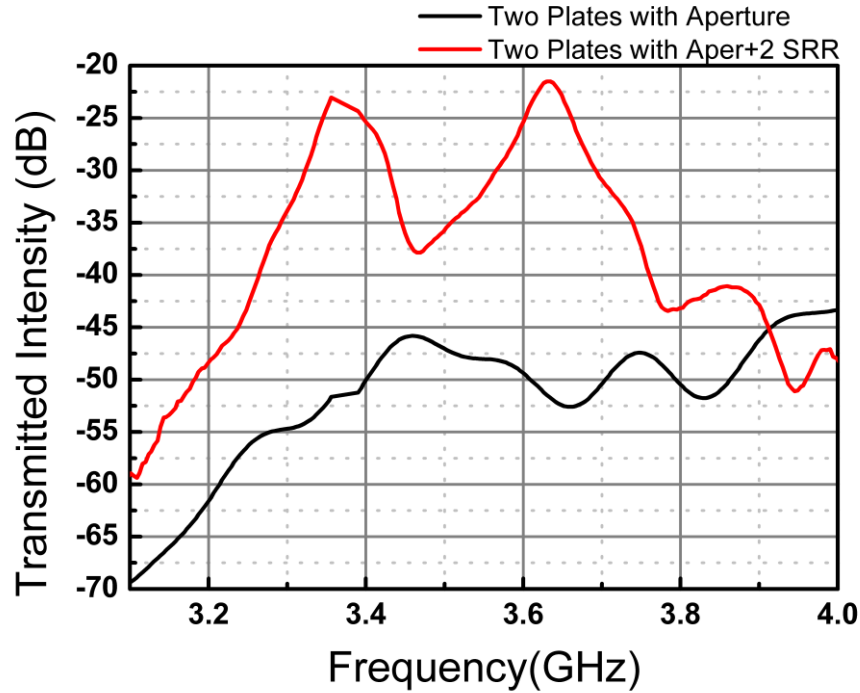


Figure 5.6: Transmission spectra of the two Stacks with two SRRs (red solid line) and two stacks without SRRs (black solid line).

In the third experiment set, we added the third plate incorporating with the SRR behind of the second plate. The third plate was placed 1.5 mm away from the second one again. The receiving antenna was shifted 3 mm away from the third metal plate as we did in second experiment set. We measured the transmission spectra of the cases with SRR and without SRR once more. The enhancement factors of the measured structures are shown in Figure 5.7. As in the figure, we obtained three enhancement peaks at 3.30 GHz, 3.51 GHz and 3.636 GHz on the order of 1484-fold, 1055-fold, and 278-fold enhancement respectively.

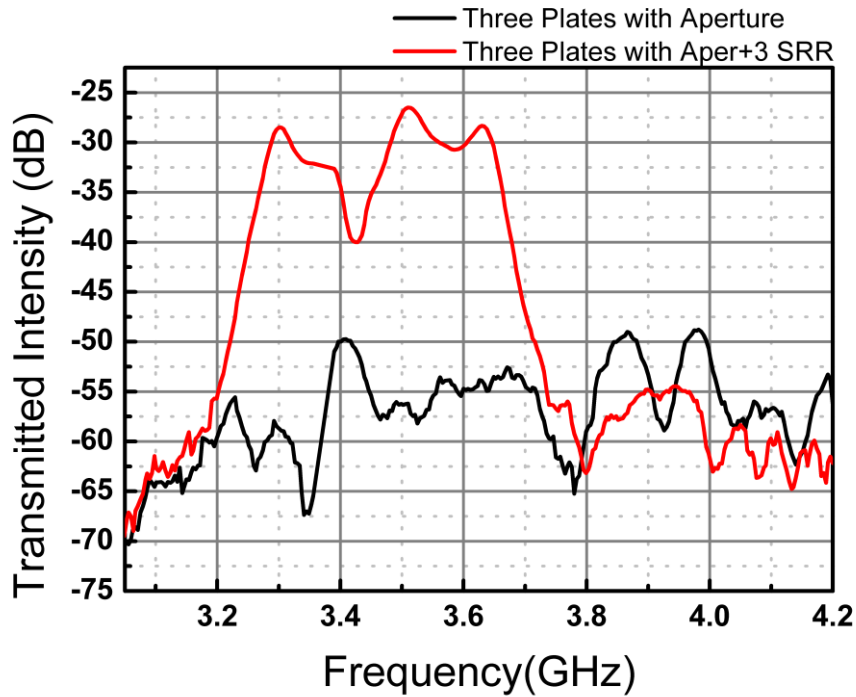


Figure 5.7: Transmission spectra of the three Stacks with three SRRs (red solid line) and three stacks without SRRs (black solid line).

Finally, the last experiment set has been carried out by adding the last plate behind the third stack. Likewise, it was placed 1.5 mm away from the third plate and the antenna was shifted 3 mm away. The transmission data are collected and enhancement results are calculated from the division of linearized S21 data of four stacks with SRRs to without SRRs. In this case, as we expected to obtain four enhancement peaks. The results are presented in Figure 5.8. The resonances were appeared at the four different frequencies as we expected that are at 3.27 GHz, 3.40 GHz, 3.54 GHz, and 3.65 GHz with 348-fold, 1482-fold, 1566-fold, and 160-fold enhancement factors.

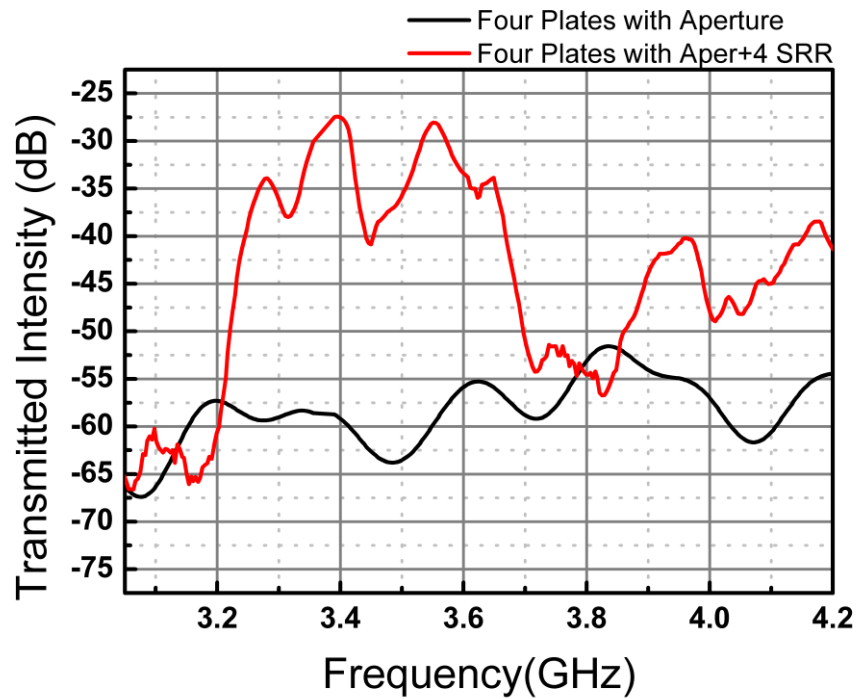


Figure 5.8: Transmission spectra of the four Stacks with four SRR (red solid line) and four stacks without SRRs (black solid line).

Moreover, to see the big picture, we have collected all of the transmission enhancement results together in one graph as shown in Figure 5.9. We observed from the graph that the more stacks (plates with SRRs) added, the wider band and the more enhancement factors are obtained.

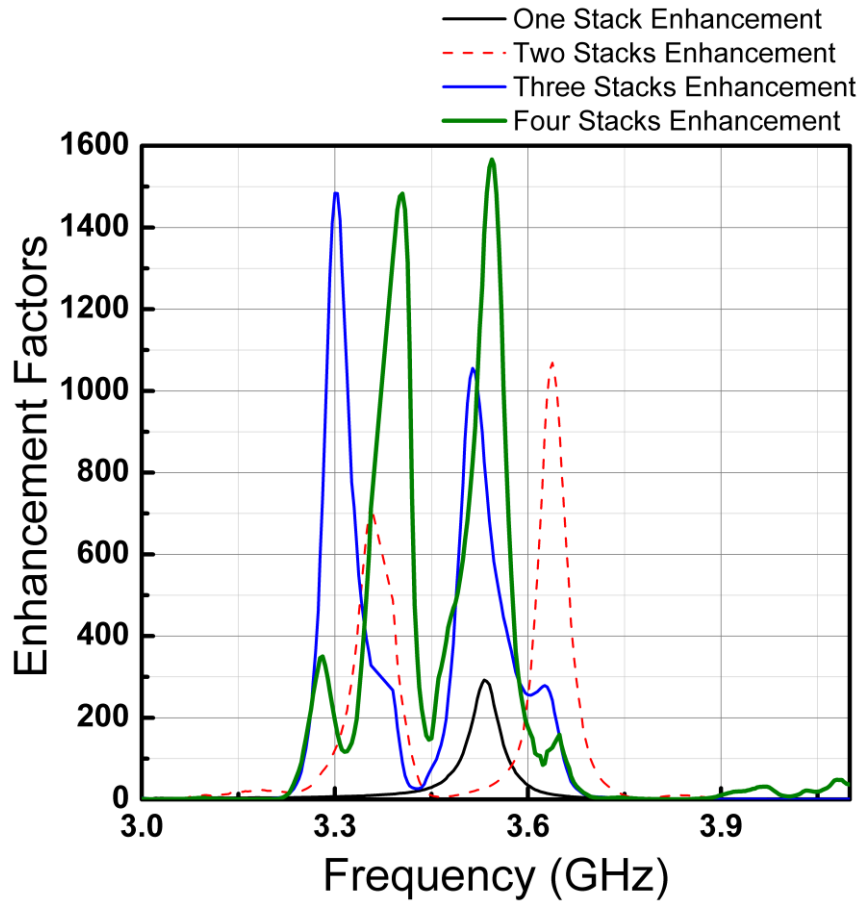


Figure 5.9: Calculated enhancement factors of single stack-SRR (solid black line), two stacks-two SRRs (dashed red line), three stacks-three SRRs (solid blue line), four stacks-four SRRs (solid green line).

The enhancement factors have increased from on the order of 300-fold to 1570-fold when the stack number is increased up to four. In addition, the range of the enhancement band increases from single frequency (3.535) to the range around 3.20 GHz to 3.65 GHz. Thus, we could achieve broader enhancement and multi-peak resonance behavior.

Although we obtained satisfying enhancement results; we still have some unexpected errors in the transmission spectra due to diffractions from the apertures and fabrication issues. The stacks used in the experiments have to be aligned perfectly. Even a tiny shift in the alignment could create enormous errors in the transmission results.

We have also verified the experimental data by numerical simulations using CST Microwave Studio. During the simulations, we stayed loyal to the experiments by preserving the same distances between the stacks and antennas. The waveguide antennas are adopted from the previously modeled antennae in Chapter 3 and Chapter 4. The dielectric constant is designed as $\epsilon = 4$, and tangent delta loss $\delta = 0.01$. The open boundary conditions are applied throughout the simulations in order to permit the diffractions. The results are shown in Figure 5.10. There is a good agreement between the experimental data and simulations.

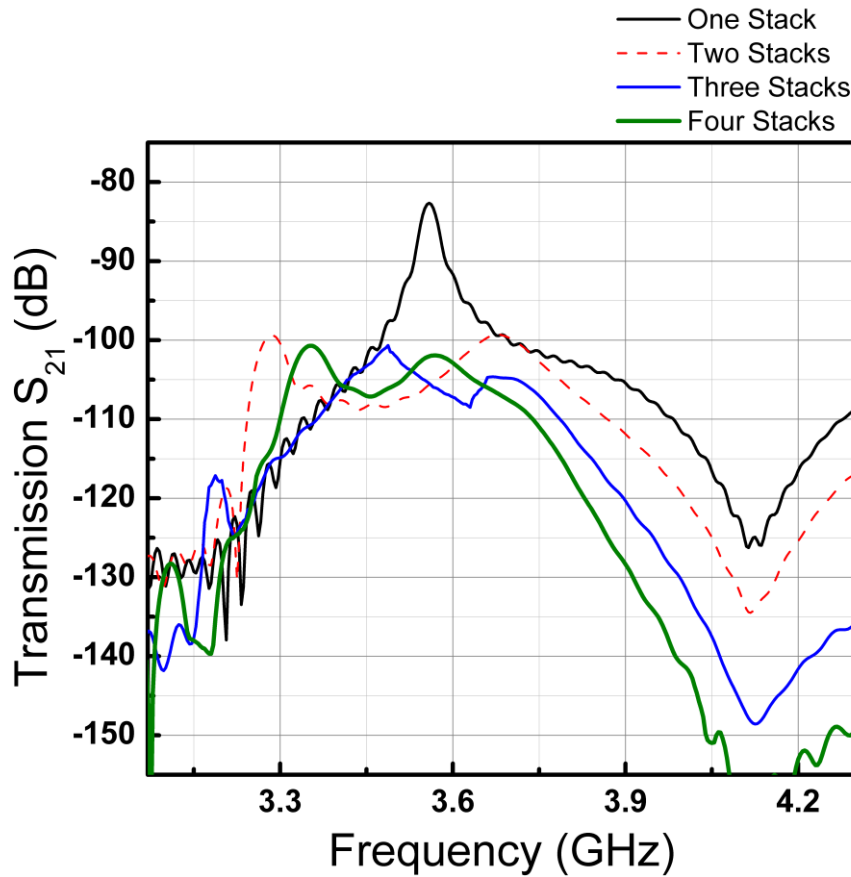


Figure 5.10: Simulated Transmission Spectra of single stack-SRR (solid black line), two stacks-two SRRs (dashed red line), three stacks-three SRRs (solid blue line), four stacks-four SRRs (solid green line).

5.3 Physical Analysis and Tight Binding Calculations

In this section, we investigated the theoretical approach of the coupling between the localized cavity modes by using Tight Binding (TB) Calculations. As we mention in the introduction of the Chapter 5, we adopted the coupled-cavity phenomenon for our experiments. Since we treat the system as coupled cavities, we can apply the TB analysis that is applied to photonic crystals. We also observed the eigenmode splitting in the coupled cavities through TB analysis.

Since the Tight Binding Method is formulated for Solid State Physics, due to similar behaviors of the photons in the evanescent mode and the impurities in Semiconductors, it is shown that it can be used for photonic crystals [54, 55]. Stefanou et al. treated photonic crystals with “impurity bands” approach [56].

To start our Tight Binding Analysis, we first inspired from the study of Yariv et al. Yariv and his colleagues applied TB methods and obtained dispersion relations and group velocity of the photonic band in *coupled-resonator optical waveguide* (CROW). They found that the CROWs are characterized by the coupling factor (κ_1) [57]. Then, recently, Bayindir et al. used the TB formalization that is used by Yariv et al. and applied to the coupled defect modes in three dimensional Photonic Crystals [58]. Bayindir et al. experimentally proposed the eigenmode splitting due to coupling of evanescent defect modes in three dimensional PC. They also obtained dispersion relations for the waveguiding band from TB calculations and phase measurements.

In this study we used the same formalization that is derived by Yariv et al. and applied to PCs by Bayindir et al. since our stack-like SRR model is analogous to coupled-cavity model. In Section 5.2, we performed the transmission experiments up to four stacks with four coupled SRRs. Using the three of them would be sufficient for us to obtain TB parameters. We applied TB formalization as Bayindir et al. used in [58] to our experimental data to calculate the TB parameters. We also applied TB approach to simulation result to demonstrate the con-

sistency with the experiment. Finally, we showed that the coupling factors from the TB calculation and 10-Stack-SRR simulations are consistent.

As we found in Section 5.2, the first defect mode occurs at $\Omega = 3.535$ GHz, and after the adding the second plate, we obtained two defect modes that occurs at $\omega_1 = 3.357$ GHz and $\omega_2 = 3.632$ GHz. Finally, we obtained three defect modes when the third plate is added such that $\Gamma_1 = 3.30$ GHz, $\Gamma_2 = 3.51$ GHz, and $\Gamma_3 = 3.636$ GHz. To understand the physics behind the splitting in the cavity modes or in a simpler term resonances, we applied the TB model to our system that is described in [57] and [58]. Here, we adopted the modeling that is introduced by these references.

According to the methods that are mentioned in [57] and [58]; we have to start by considering Maxwell's Equations. Let us denote Electric Field as $E_\Omega(\mathbf{r})$ as in the references. Corresponding Maxwell's equation can be formed as:

$$\nabla \times [\nabla \times E_\Omega(\mathbf{r})] = \epsilon_0(\mathbf{r})(\Omega/c)^2 E_\Omega(\mathbf{r}) \quad (3)$$

According to the equation above; $\epsilon_0(\mathbf{r})$ is the dielectric constant of a single defect (or resonance peak, cavity) and Ω is the eigenfrequency. Likewise, when we consider two-peaks system, the eigenmode consists of two individual evanescent mode: $E_\Omega(\mathbf{r})$ and $E_\Omega(\mathbf{r} - \mathbf{ax})$, where \mathbf{a} is the intercavity distance which is the distance between the two stacks in our case. Two individual evanescent modes are as follows:

$$E_\omega(\mathbf{r}) = AE_\Omega(\mathbf{r}) + BE_\Omega(\mathbf{r} - \mathbf{ax}) \quad (4)$$

The newly introduced eigenmode $E_\omega(\mathbf{r})$, $\epsilon_0(\mathbf{r} - \mathbf{ax})$ and Ω inserted the Maxwell equation specified as Equation 3. Also, multiplying both sides from the left first by $E_\Omega(\mathbf{r})$ and $E_\Omega(\mathbf{r})$, we can obtain the following new equation:

$$\omega_{1,2}^2 = \Omega^2(1 \pm \beta_1)/(1 \pm \alpha_1 + \Delta\alpha) \quad (5)$$

Hence, the TB parameters α_1 and β_1 can be calculated by inserting ω_1 , ω_2 and Ω . The $\Delta\alpha$ is assumed to be negligible comparing to α_1 and β_1 . Therefore, we

inserted $\omega_1 = 3.357$ GHz, $\omega_2 = 3.632$ GHz, and $\Omega = 3.535$ GHz. Then, we found $\alpha_1 = -0.2768$ and $\beta_1 = -0.3486$.

For the three coupled defect system, the major eigenfrequency Ω is split into three resonances Γ_1 , Γ_2 , and Γ_3 .

$$\Gamma_2^2 \approx \Omega^2 \tag{6}$$

$$\Gamma_{1,3}^2 \approx \Omega^2 (1 \pm \sqrt{2} \beta_1) / (1 \pm \sqrt{2} \alpha_1) \tag{7}$$

Inserting the TB parameters α_1 , β_1 and Ω that we found in Equation (5), we calculated Γ_1 , Γ_2 , and Γ_3 as 3.23 GHz, 3.53 GHz, and 3.66 GHz respectively. The calculated resonance frequencies and measured results are exhibited in Table 5.1.

	Calculated (GHz)	Measured (GHz)
Γ_1	3.2304	3.30
Γ_2	3.536	3.51
Γ_3	3.6603	3.63

Table 5.1: Calculated and measured values of resonant frequencies for the Three Stack – Three SRR system.

As we can see from Table 5.1, the calculated resonance frequencies by Tight Binding approach fit very well with the measured resonance frequencies. The calculated results also satisfy the validity of the experimental results.

To be more convinced, we applied the TB approach to the simulation results. We could not use more than four plates due to fabrication difficultness and experimental conditions. We needed 10-stacks results to find the coupling factor. However, we could realize with the simulations. Since simulation and measurements results coincide, we simulated the same structure with more stacks. We men-

tioned the single defect model, two split evanescent defect modes, and three split evanescent defect modes are obtained in the simulations.

According to these simulation results, we recalculate the TB parameters once more. So, we inserted $\omega_1 = 3.285$ GHz, $\omega_2 = 3.678$ GHz, and $\Omega = 3.5586$ GHz. Then, we found $\alpha_1 = -0.3686$ and $\beta_1 = -0.4620$.

For the three coupled defect system, the major eigenfrequency Ω is split into three resonances Γ_1 , Γ_2 , and Γ_3 . The calculated resonance frequencies and measured results are exhibited in Table 5.2.

	Calculated (GHz)	Simulated (GHz)
Γ_1	3.0282	3.18
Γ_2	3.5586	3.49
Γ_3	3.70	3.68

Table 5.2: The calculated and simulated values of resonant frequencies for the Three Stack –Three SRR system.

Since, the simulation results and experimental results have a good matching, for the next analysis; we treated the simulation results as experimental results. For the case of a periodic defect array, the eigenmode can be calculated as the linear combination of each defect modes:

$$E(\mathbf{r}) = E_0 \sum \exp(-in\mathbf{k}a) E_{\Omega}(\mathbf{r} - n\mathbf{a}x) \quad (8)$$

Using Equations (3) and (8), the dispersion relation can be obtained as follows:

$$\omega^2(\mathbf{k}) = \omega^2 \frac{1 + 2\beta_1 \cos(\mathbf{k}a)}{1 + \Delta\alpha + 2\alpha_1 \cos(\mathbf{k}a)} \quad (9)$$

If α_1 and β_1 TB parameters are smaller compared to 1, we can neglect them. Thus, the Equation (9) is simplified in a form:

$\omega(\mathbf{k}) \approx \Omega + \Omega (\beta_1 - \alpha_1) \cos(\mathbf{k}a)$ and let $\kappa_1 = \beta_1 - \alpha_1$, and according to the calculated TB parameters from the simulations, $\kappa_1 = -0.0934$.

Finally, we simulated the ten defect structure (ten-stacked plates with SRRs) to form a wide defect band as shown in Figure 5.11. The graph has a band from 3.05 GHz to 3.75 GHz. The bandwidth of the transmission band is $\Delta\omega = 0.70$. The parameter κ_1 can be obtained from the waveguiding bandwidth:

$|\kappa_1| = \Delta\omega / 2\Omega \approx 0.0984$, which is almost the same as we found by the difference of β_1 and α_1 from the coupling of two defect modes.

As a conclusion, in this study we first observed that the SRR coupled an aperture design in the stacks form is analogous to coupled cavity PC or metamaterials. As impurity states are analyzed with TB methods in semiconductors, the photonic bands can also be analyzed with TB methods in photonic crystals. Our model adopted the coupled-cavity model, hence we could analyze with TB methods. We achieved to have consistent calculations with TB methods. Finally, we calculated the coupling factors which were calculated from the calculations of TB parameters and from the 10-Stack simulation results. The both coupling factors were consistent with each other.

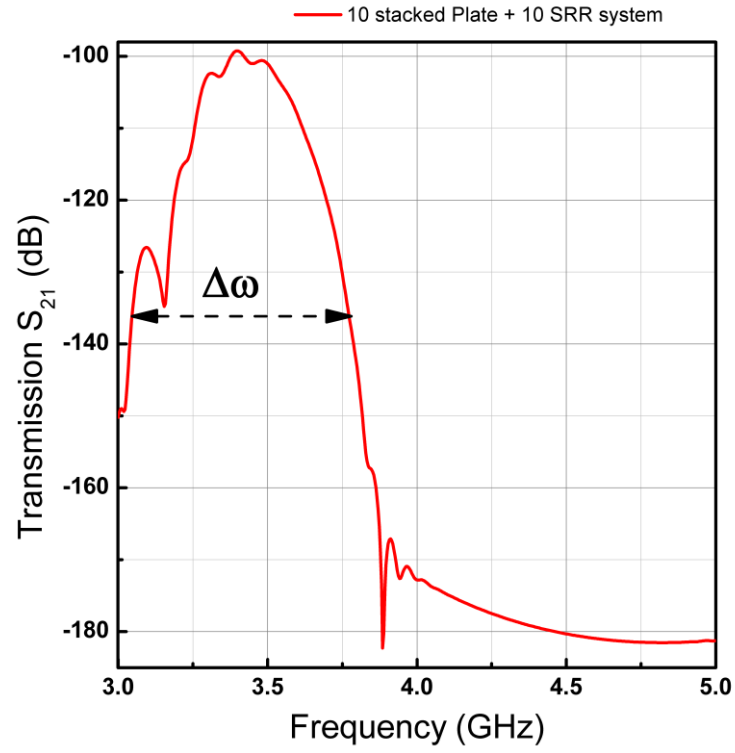


Figure 5.11: Simulated Transmission spectrum of the ten stack-ten SRRs system with showing the enhanced band gap $\Delta\omega$.

Chapter 6

Conclusion

The aim of this thesis is to present alternative approaches that offer higher transmission enhancement results than previously works in the literature. We performed transmission enhancement experiments and verified them by numerical simulations. We investigated the physical origins of the transmission enhancement. The reported results in this thesis are promising for the future studies.

We first introduced the theoretical backgrounds for the metamaterials and transmission through subwavelength holes. We first studied the major building blocks of metamaterials that are *Split Ring Resonators*. We discussed the resonant behavior of the SRRs from the circuit theory point of view. Then, we introduced the transmission through subwavelength holes and the efficiency is dependent to radius of the aperture and operational wavelength. We also gave brief information about the previous designs in order to increase transmission efficiency such as periodic array of holes, periodic corrugations, and metamaterial coupled aperture systems. Finally, we introduced the challenges that we need to overcome.

Then, we proposed an alternative design that consists of Connected Split Ring Resonators (CSRR) inserted across the subwavelength aperture. We performed the experiments and verified the results by numerical simulations. In the experiments, we obtained more than 70,000-fold enhancement factor which was the highest factor among other reported results until that study. Also, we investigated the physical origins of the enhancement and magnetic resonance. We first shorted the inner and outer rings of the CSRR. We observed that when the inner rings were shorted, the magnetic resonance remains, conversely when the outer ring were shorted, the magnetic resonance disappeared. We also showed the aperture independency of the resonance frequency. Then, we compared the CSRR

CHAPTER 6. CONCLUSION

with the previous SRR designs and discuss the significance of the connecting bars. Finally, we analyzed the enhancement by induced surface currents and field localization.

Furthermore, we designed SRRs with Omega particles which are called Omega-like SRRs. We expected to surpass the enhancement results that we found in Chapter 3 due to their bi-anisotropic, pseudo-chiral and low loss nature. We performed the experiments and numerical analysis. We obtained more than 150,000-fold enhancement which is even higher than the previous results that we achieved in Chapter 4. We also did the parametrical analysis. We first omit the Omega sample on the one side of the PCB and we observed that the resonant behavior is weakened. Finally, we analyzed the surface currents to understand the physical origins of the two enhancement peaks. We observed that we have two modes that are even and odd mode. These modes affect the coupling between the loops and connecting arms.

Then, instead of using single plate with an SRR, we used stacks of metal plates with SRRs. We aimed to obtain a multi-peak resonant transmission. We started our experiments with a single plate inserted with a conventional SRR which we obtained a single peak. Then we used two stacks with two SRR, in which we obtained two enhancement peaks. We measured three stacks with three SRR and obtained three enhancement peaks. Finally we obtained four enhancement peaks with four stacks with four SRRs as we expected. As we add more stack, we obtained higher and broader enhancement. Lastly, we applied the Tight Binding analysis to understand physical origins of the enhancement characteristics. The measurement and simulations data were consistent as well as TB calculations.

In this thesis, we showed that the CSRR, Omega-like and Stack-like SRR designs can be used in many applications depending on the desired band structures such as narrow band high transmission, wide band multi-peak transmissions. Also these different SRR configurations can be designed in smaller scales in order to shift the resonance frequencies to optical regimes. Hence, they can be adapted to many applications including imaging, perfect lenses, lithography,

CHAPTER 6. CONCLUSION

biosensing and other photonic applications using micro and nano-fabrication techniques.

BIBLIOGRAPHY

- [1] V. G. Veselago, "The electrodynamics of substances with simultaneously negative values of ϵ and μ ," *Physics-Uspekhi*, vol. 10, pp. 509-514, 1968.
- [2] J. Pendry, A. Holden, D. Robbins, and W. Stewart, "Magnetism from conductors and enhanced nonlinear phenomena," *Microwave Theory and Techniques, IEEE Transactions on*, vol. 47, pp. 2075-2084, 1999.
- [3] H. Caglayan, I. Bulu, and O. Ekmel, "Plasmonic structures with extraordinary transmission and highly directional beaming properties," *Microwave and Optical Technology Letters*, vol. 48, pp. 2491-2496, 2006.
- [4] H. Caglayan, I. Bulu, and E. Ozbay, "Beaming of electromagnetic waves emitted through a subwavelength annular aperture," *JOSA B*, vol. 23, pp. 419-422, 2006.
- [5] H. Lezec, A. Degiron, E. Devaux, R. Linke, L. Martin-Moreno, F. Garcia-Vidal, and T. Ebbesen, "Beaming light from a subwavelength aperture," *Science*, vol. 297, pp. 820-822, 2002.
- [6] J. B. Pendry, "Negative refraction makes a perfect lens," *Physical Review Letters*, vol. 85, pp. 3966-3969, 2000.
- [7] D. Schurig, J. Pendry, and D. Smith, "Transformation-designed optical elements," *Opt. Express*, vol. 15, pp. 14772-14782, 2007.
- [8] D. Schurig, J. Mock, B. Justice, S. A. Cummer, J. Pendry, A. Starr, and D. Smith, "Metamaterial electromagnetic cloak at microwave frequencies," *Science*, vol. 314, pp. 977-980, 2006.
- [9] E. Ozbay, "Plasmonics: merging photonics and electronics at nanoscale dimensions," *Science*, vol. 311, pp. 189-193, 2006.

- [10] S. Linden, C. Enkrich, M. Wegener, J. Zhou, T. Koschny, and C. M. Soukoulis, "Magnetic response of metamaterials at 100 terahertz," *Science*, vol. 306, pp. 1351-1353, 2004.
- [11] G. Dolling, C. Enkrich, M. Wegener, C. M. Soukoulis, and S. Linden, "Simultaneous negative phase and group velocity of light in a metamaterial," *Science*, vol. 312, pp. 892-894, 2006.
- [12] K. Aydin, K. Guven, M. Kafesaki, L. Zhang, C. M. Soukoulis, and E. Ozbay, "Experimental observation of true left-handed transmission peaks in metamaterials," *Optics letters*, vol. 29, pp. 2623-2625, 2004.
- [13] K. Guven, K. Aydin, and E. Ozbay, "Experimental analysis of true left-handed behaviour and transmission properties of composite metamaterials," *Photonics and Nanostructures-Fundamentals and Applications*, vol. 3, pp. 75-78, 2005.
- [14] H. Bethe, "Theory of diffraction by small holes," *Physical Review*, vol. 66, pp. 163-182, 1944.
- [15] C. Genet and T. Ebbesen, "Light in tiny holes," *Nature*, vol. 445, pp. 39-46, 2007.
- [16] T. W. Ebbesen, H. Lezec, H. Ghaemi, T. Thio, and P. Wolff, "Extraordinary optical transmission through sub-wavelength hole arrays," *Nature*, vol. 391, pp. 667-669, 1998.
- [17] L. Martin-Moreno, F. Garcia-Vidal, H. Lezec, K. Pellerin, T. Thio, J. Pendry, and T. Ebbesen, "Theory of extraordinary optical transmission through subwavelength hole arrays," *Physical Review Letters*, vol. 86, pp. 1114-1117, 2001.
- [18] J. Porto, F. Garcia-Vidal, and J. Pendry, "Transmission resonances on metallic gratings with very narrow slits," *Physical Review Letters*, vol. 83, pp. 2845-2848, 1999.
- [19] J. Bravo-Abad, A. Degiron, F. Przybilla, C. Genet, F. J. García-Vidal, L. Martín-Moreno, and T. Ebbesen, "How light emerges from an illuminated array of subwavelength holes," *Nature Physics*, vol. 2, pp. 120-123, 2006.

- [20] K. Lee and Q. H. Park, "Coupling of surface plasmon polaritons and light in metallic nanoslits," *Physical Review Letters*, vol. 95, p. 103902, 2005.
- [21] H. Schouten, N. Kuzmin, G. Dubois, T. Visser, G. Gbur, P. Alkemade, H. Blok, G. W. Hooft, D. Lenstra, and E. Eliel, "Plasmon-assisted two-slit transmission: Young's experiment revisited," *Physical Review Letters*, vol. 94, p. 53901, 2005.
- [22] A. Dogariu, T. Thio, L. Wang, T. Ebbesen, and H. Lezec, "Delay in light transmission through small apertures," *Optics letters*, vol. 26, pp. 450-452, 2001.
- [23] Q. Wang, J. Li, C. Huang, C. Zhang, and Y. Zhu, "Enhanced optical transmission through metal films with rotation-symmetrical hole arrays," *Applied physics letters*, vol. 87, p. 091105, 2005.
- [24] W. L. Barnes, W. A. Murray, J. Dintinger, E. Devaux, and T. Ebbesen, "Surface plasmon polaritons and their role in the enhanced transmission of light through periodic arrays of subwavelength holes in a metal film," 2004.
- [25] K. J. K. Koerkamp, S. Enoch, F. Segerink, N. Van Hulst, and L. Kuipers, "Strong influence of hole shape on extraordinary transmission through periodic arrays of subwavelength holes," *Physical Review Letters*, vol. 92, p. 183901, 2004.
- [26] T. Matsui, A. Agrawal, A. Nahata, and Z. V. Vardeny, "Transmission resonances through aperiodic arrays of subwavelength apertures," *Nature*, vol. 446, pp. 517-521, 2007.
- [27] H. Ghaemi, T. Thio, D. Grupp, T. W. Ebbesen, and H. Lezec, "Surface plasmons enhance optical transmission through subwavelength holes," *Physical Review B*, vol. 58, p. 6779, 1998.
- [28] F. J. G. de Abajo, "Light transmission through a single cylindrical hole in a metallic film," *Opt. Express*, vol. 10, pp. 1475-1484, 2002.

- [29] A. Zakharian, M. Mansuripur, and J. Moloney, "Transmission of light through small elliptical apertures," *Optics Express*, vol. 12, pp. 2631-2648, 2004.
- [30] F. Garcia-Vidal, E. Moreno, J. Porto, and L. Martin-Moreno, "Transmission of light through a single rectangular hole," *Physical Review Letters*, vol. 95, p. 103901, 2005.
- [31] L. Yin, V. Vlasko-Vlasov, A. Rydh, J. Pearson, U. Welp, S. H. Chang, S. Gray, G. Schatz, D. Brown, and C. Kimball, "Surface plasmons at single nanoholes in Au films," *Applied physics letters*, vol. 85, p. 467, 2004.
- [32] A. Degiron and T. Ebbesen, "Analysis of the transmission process through single apertures surrounded by periodic corrugations," *Optics Express*, vol. 12, pp. 3694-3700, 2004.
- [33] F. Garcia-Vidal, L. Martin-Moreno, H. Lezec, and T. Ebbesen, "Focusing light with a single subwavelength aperture flanked by surface corrugations," *Applied physics letters*, vol. 83, pp. 4500-4502, 2003.
- [34] J. Pendry, L. Martin-Moreno, and F. Garcia-Vidal, "Mimicking surface plasmons with structured surfaces," *Science*, vol. 305, pp. 847-848, 2004.
- [35] F. Garcia-Vidal, L. Martin-Moreno, and J. Pendry, "Surfaces with holes in them: new plasmonic metamaterials," *Journal of Optics A: Pure and Applied Optics*, vol. 7, p. S97, 2005.
- [36] A. Alù, F. Bilotti, N. Engheta, and L. Vegni, "Subwavelength planar leaky-wave components with metamaterial bilayers," *Antennas and Propagation, IEEE Transactions on*, vol. 55, pp. 882-891, 2007.
- [37] R. Marqués, F. Mesa, J. Martel, and F. Medina, "Comparative analysis of edge-and broadside-coupled split ring resonators for metamaterial design-theory and experiments," *Antennas and Propagation, IEEE Transactions on*, vol. 51, pp. 2572-2581, 2003.
- [38] K. Aydin, A. O. Cakmak, L. Sahin, Z. Li, F. Bilotti, L. Vegni, and E. Ozbay, "Split-ring-resonator-coupled enhanced transmission through a

- single subwavelength aperture," *Physical Review Letters*, vol. 102, p. 13904, 2009.
- [39] A. O. Cakmak, K. Aydin, E. Colak, Z. Li, F. Bilotti, L. Vegni, and E. Ozbay, "Enhanced transmission through a subwavelength aperture using metamaterials," *Applied physics letters*, vol. 95, p. 052103, 2009.
- [40] M. M. I. Saadoun and N. Engheta, "A reciprocal phase shifter using novel pseudochiral or Ω medium," *Microwave and Optical Technology Letters*, vol. 5, pp. 184-188, 1992.
- [41] C. Simovski, S. Tretyakov, A. Sochava, B. Sauviac, F. Mariotte, and T. Kharina, "Antenna model for conductive omega particles," *Journal of electromagnetic waves and applications*, vol. 11, pp. 1509-1530, 1997.
- [42] C. R. Simovski and S. He, "Frequency range and explicit expressions for negative permittivity and permeability for an isotropic medium formed by a lattice of perfectly conducting [Omega] particles," *Physics letters A*, vol. 311, pp. 254-263, 2003.
- [43] L. Ran, J. Huangfu, H. Chen, Y. Li, X. Zhang, K. Chen, and J. Kong, "Microwave solid-state left-handed material with a broad bandwidth and an ultralow loss," *Physical Review B*, vol. 70, p. 073102, 2004.
- [44] K. Aydin, Z. Li, S. Bilge, and E. Ozbay, "Experimental and numerical study of omega type bianisotropic metamaterials combined with a negative permittivity medium," *Photonics and Nanostructures-Fundamentals and Applications*, vol. 6, pp. 116-121, 2008.
- [45] D. Ates, A. O. Cakmak, E. Colak, R. Zhao, C. Soukoulis, and E. Ozbay, "Transmission enhancement through deep subwavelength apertures using connected split ring resonators," *Optics Express*, vol. 18, pp. 3952-3966, 2010.
- [46] D. Ates, A. O. Cakmak, and E. Ozbay, "Near-field light localization using subwavelength apertures incorporated with metamaterials," *Optics Communications*, 2012.
- [47] E. Ozbay, K. Aydin, E. Cubukcu, and M. Bayindir, "Transmission and reflection properties of composite double negative metamaterials in free

- space," *Antennas and Propagation, IEEE Transactions on*, vol. 51, pp. 2592-2595, 2003.
- [48] K. Guven and E. Ozbay, "Coupling and phase analysis of cavity structures in two-dimensional photonic crystals," *Physical Review B*, vol. 71, p. 085108, 2005.
- [49] E. Ozbay, M. Bayindir, I. Bulu, and E. Cubukcu, "Investigation of localized coupled-cavity modes in two-dimensional photonic bandgap structures," *Quantum Electronics, IEEE Journal of*, vol. 38, pp. 837-843, 2002.
- [50] M. Bayindir, C. Kural, and E. Ozbay, "Coupled optical microcavities in one-dimensional photonic bandgap structures," *Journal of Optics A: Pure and Applied Optics*, vol. 3, p. S184, 2001.
- [51] H. Caglayan, I. Bulu, M. Loncar, and E. Ozbay, "Observation of coupled-cavity structures in metamaterials," *Applied physics letters*, vol. 93, pp. 121910-121910-3, 2008.
- [52] H. Caglayan, I. Bulu, M. Loncar, and E. Ozbay, "Experimental observation of cavity formation in composite metamaterials," *Optics Express*, vol. 16, pp. 11132-11140, 2008.
- [53] H. Caglayan, I. Bulu, M. Loncar, and E. Ozbay, "Cavity formation in split ring resonators," *Photonics and Nanostructures-Fundamentals and Applications*, vol. 6, pp. 200-204, 2008.
- [54] N. W. Ashcroft and N. D. Mermin, "Solid State Physics (Saunders College, Philadelphia, 1976)," *Author Affiliations LC Botten University of Technology, Sydney RA Hansen, C. Martijn de Sterke University of Sydney Cited By OSA is able to provide readers links to articles that cite this paper by participating in CrossRef's Cited-By Linking service. CrossRef includes content from more than*, vol. 3000, 2010.
- [55] J. C. Slater and G. Koster, "Simplified LCAO method for the periodic potential problem," *Physical Review*, vol. 94, p. 1498, 1954.
- [56] N. Stefanou and A. Modinos, "Impurity bands in photonic insulators," *Physical Review B*, vol. 57, p. 12127, 1998.

- [57] A. Yariv, Y. Xu, R. K. Lee, and A. Scherer, "Coupled-resonator optical waveguide: a proposal and analysis," *Optics letters*, vol. 24, pp. 711-713, 1999.
- [58] M. Bayindir, B. Temelkuran, and E. Ozbay, "Tight-binding description of the coupled defect modes in three-dimensional photonic crystals," *Physical Review Letters*, vol. 84, pp. 2140-2143, 2000.